Atmos. Chem. Phys. Discuss., 15, 32469–32518, 2015
www.atmos-chem-phys-discuss.net/15/32469/2015/
doi:10.5194/acpd-15-32469-2015

Atmospheric Chemistry and Physics Discussions

Mapping pan-Arctic methane emissions at high spatial resolution using an adjoint atmospheric transport and inversion method and process-based wetland and lake biogeochemical models

Z. Tan[1,2], Q. Zhuang[1,2,3], D. K. Henze[4], C. Frankenberg[5], E. Dlugokencky[6], C. Sweeney[6], and A. J. Turner[7]

[1]Department of Earth, Atmospheric, and Planetary Sciences, Purdue University, West Lafayette, Indiana, USA
[2]Purdue Climate Change Research Center, Purdue University, West Lafayette, Indiana, USA
[3]Department of Agronomy, Purdue University, West Lafayette, Indiana, USA
[4]Department of Mechanical Engineering, University of Colorado, Boulder, Colorado, USA
[5]Jet Propulsion Laboratory, California Institute of Technology, Pasadena, California, USA
[6]Global Monitoring Division, NOAA Earth System Research Laboratory, Boulder, Colorado, USA

[7]School of Engineering and Applied Sciences, Harvard University, Cambridge, Massachusetts, USA

Received: 19 October 2015 – Accepted: 8 November 2015 – Published: 18 November 2015

Correspondence to: Q. Zhuang (qzhuang@purdue.edu)

Published by Copernicus Publications on behalf of the European Geosciences Union.

ACPD
15, 32469–32518, 2015

Abstract

Understanding methane emissions from the Arctic, a fast warming carbon reservoir, is important for projecting changes in the global methane cycle under future climate scenarios. Here we optimize Arctic methane emissions with a nested-grid high-resolution inverse model by assimilating both high-precision surface measurements and column-average SCIAMACHY satellite retrievals of methane mole fraction. For the first time, methane emissions from lakes are integrated into an atmospheric transport and inversion estimate, together with prior wetland emissions estimated by six different biogeochemical models. We find that, the global methane emissions during July 2004–June 2005 ranged from 496.4 to 511.5 $Tg\,yr^{-1}$, with wetland methane emissions ranging from 130.0 to 203.3 $Tg\,yr^{-1}$. The Arctic methane emissions during July 2004–June 2005 were in the range of 14.6–30.4 $Tg\,yr^{-1}$, with wetland and lake emissions ranging from 8.8 to 20.4 $Tg\,yr^{-1}$ and from 5.4 to 7.9 $Tg\,yr^{-1}$ respectively. Canadian and Siberian lakes contributed most of the estimated lake emissions. Due to insufficient measurements in the region, Arctic methane emissions are less constrained in northern Russia than in Alaska, northern Canada and Scandinavia. Comparison of different inversions indicates that the distribution of global and Arctic methane emissions is sensitive to prior wetland emissions. Evaluation with independent datasets shows that the global and Arctic inversions improve estimates of methane mixing ratios in boundary layer and free troposphere. The high-resolution inversions provide more details about the spatial distribution of methane emissions in the Arctic.

1 Introduction

Methane (CH_4) is an important long-lived atmospheric trace gas. It is the second most powerful carbon-based greenhouse gas in the atmosphere behind carbon dioxide (CO_2) and also plays a significant role in the cycles of ozone (O_3), hydroxyl radicals (OH) and stratospheric water vapor (H_2O) (Myhre et al., 2013; Shindell et al., 2009).

ACPD
15, 32469–32518, 2015

The atmospheric burden of CH_4 is now more than factor of 2.5 greater than the pre-industrial value of about 700 ppb (Etheridge et al., 1998), mainly due to anthropogenic emissions. Major sources and sinks of CH_4 have been identified (Denman et al., 2007); however their individual strengths and the causes of the observed concentration trends and inter-annual fluctuations are not well known. For instance, scientists have not yet agreed on what caused the leveling off of atmospheric CH_4 since the 1980s (Dlugokencky et al., 2003; Bousquet et al., 2006; Aydin et al., 2011; Kai et al., 2011; Levin et al., 2012; Simpson et al., 2012; Kirschke et al., 2013) and the recent rebounding of its growth since 2007 (Rigby et al., 2008; Dlugokencky et al., 2009; Nisbet et al., 2014).

Given the uncertainty regarding drivers of trends in CH_4 concentrations, much effort has focused on refining estimates of CH_4 sources using one of two types of general approaches for estimating the contribution of individual CH_4 sources or sinks to the overall CH_4 budget: "bottom-up" and "top-down" methods. Bottom-up estimates are scaled up from small scale studies of emissions factors (e.g., CH_4 flux) and activity data (e.g., global area that applies to the particular wetland studied) or from biogeochemical models (e.g. wetlands) with environmental conditions (Fung et al., 1991; Zhuang et al., 2004; Walter et al., 2006; Tan and Zhuang, 2015a, b). In contrast, top-down estimates use in situ and satellite observations of CH_4 that are representative of large spatial scales with a chemical transport model (CTM) to infer strengths of CH_4 sources and sinks (e.g., Enting, 2002; Bergamaschi et al., 2009). In Bayesian theory, a top-down estimate can reduce uncertainty in bottom-up inventories through the use of model and ambient observations. This method, called Bayesian inference, has been successfully employed in numerous studies for estimating the global CH_4 budget at coarse spatial resolutions (over 300 km) (Bergamaschi et al., 2007, 2009, 2013; Meirink et al., 2008; Cressot et al., 2014; Houweling et al., 2014; Alexe et al., 2015). Many of these studies have assimilated space-borne observations of atmospheric CH_4 concentrations to constrain CH_4 emissions because they deliver dense and continuous coverage unachievable by surface networks or aircraft campaigns (Bergamaschi et al., 2007). There are two types of nadir satellite CH_4 retrievals: one from solar backscatter in the

ACPD
15, 32469–32518, 2015

shortwave infrared (SWIR) and the other from thermal infrared radiation (TIR). Between them, SWIR retrievals were more widely used in atmospheric inversion of CH_4 emissions (Bergamaschi et al., 2007, 2009, 2013; Fraser et al., 2013; Cressot et al., 2014; Houweling et al., 2014; Monteil et al., 2014; Wecht et al., 2014; Alexe et al., 2015; Turner et al., 2015) because they can provide column concentrations with near-uniform vertical sensitivity down to the surface. However, partly owing to their resolution, such coarse-resolution global inversions have not been able to constrain the strength of different CH_4 sources and the locations of CH_4 flux hotspots (Fung et al., 1991; Wecht et al., 2014). To address this issue, regional inverse models at fine spatial resolutions were developed (Miller et al., 2013; Wecht et al., 2014; Thompson et al., 2015). For example, Wecht et al. (2014) and Turner et al. (2015) have used the $1/2^{\circ} \times 2/3^{\circ}$ horizontal resolution GEOS-Chem adjoint model to constrain CH_4 emissions over North America.

Estimating CH_4 emissions from the Arctic is important for understanding the global carbon cycle because the fast warming of Arctic permafrost, one of the largest organic carbon reservoirs (Tarnocai et al., 2009), could lead to a rapid rise of CH_4 emissions (Zhuang et al., 2006; Walter et al., 2007; Koven et al., 2011). Natural sources dominate the Arctic CH_4 inventory (Fisher et al., 2011), e.g. wetlands (McGuire et al., 2012), lakes (Walter et al., 2006; Bastviken et al., 2011), sea shelves (Shakhova et al., 2013) and oceans (Kort et al., 2012). As the factors governing natural CH_4 production (methanogenesis) and oxidation (methanotrophy) are notoriously heterogeneous, estimates of Arctic CH_4 emissions are still poorly constrained, even with decades of site-level and modeling studies (Zhuang et al., 2004; Bastviken et al., 2011; Schuur et al., 2015; Tan and Zhuang, 2015a, b). And previous CH_4 inversions over the Arctic only assimilated surface measurements that were too sparse to provide constraints for fine-scale CH_4 fluxes. Further, an important consideration is specification of realistic prior fluxes, given the ill-posed nature of trace-gas inversions (Kaminski and Heimann, 2001). While CH_4 emissions from lakes could be of comparable magnitude to CH_4 emissions from wetlands in the Arctic (Walter et al., 2006, 2007; Bastviken et al., 2011; Tan and Zhuang,

ACPD
15, 32469–32518, 2015

2015a), this source has not been included in past global or regional inverse modeling studies.

To address these issues, this study uses the adjoint of a 3-D chemical transport model at high spatial resolution (less than 60 km) with the integration of both process-based wetland and lake biogeochemical models and atmospheric CH_4 mixing fractions to improve the quantification of Arctic CH_4 emissions for July 2004–June 2005. For the first time, we include CH_4 emissions from lakes in a high-resolution Bayesian inversion of CH_4 fluxes in the Arctic. As wetland emissions are likely the largest Arctic CH_4 source, this study also considers the sensitivity of our inversion to prior wetland fluxes. Section 2 describes the satellite retrievals and surface CH_4 observations that are used to infer CH_4 fluxes and evaluate posterior estimates. Section 3 describes the details of the biogeochemical models for wetland and lake emissions (Sect. 3.1), the Arctic nested-grid chemical transport model and the prior budgets of other CH_4 sources and sinks (Sect. 3.2) and the adjoint-based inversion method (Sect. 3.3). Section 4 presents the posterior CH_4 emissions and their evaluation.

2 Observations

2.1 Satellite retrievals

SWIR CH_4 retrievals are available from SCanning Imaging Absorption spectroMeter for Atmospheric CHartogrphY (SCAMACHY) for 2003–2012 (Frankenberg et al., 2006, 2008, 2011) and Greenhouse Gases Observing SATellite (GOSAT) for 2009 to present (Parker et al., 2011). SCIAMACHY, aboard the European Space Agency's environmental research satellite ENVISAT retrieves column-averaged CH_4 mixing ratios (XCH_4) from the SWIR nadir spectra (channel 6: 1.66–1.67 µm) using the IMAP-DOAS algorithm (Frankenberg et al., 2006, 2008, 2011). The satellite operates in a near polar, sun-synchronous orbit at an altitude of 800 km. At channel 6, the ground pixel size of the retrievals is about 30 km (along-track) × 60 km (across-track). We use version 6.0

ACPD
15, 32469–32518, 2015

proxy CH_4 retrievals from Frankenberg et al. (2011) that provide a weighted column average dry-mole fraction of CH_4 with 10-layer averaging kernels and prior CH_4 profiles. The averaging kernels show near-uniform vertical sensitivity in the troposphere and declining sensitivity above the tropopause (Butz et al., 2010). Some auxiliary data, e.g. the air mass factor A_F ($A_F = 1/\cos\theta + 1\cos\xi$, where θ is the solar zenith angle and ξ is the viewing angle of the satellite), water column density and dry air column density, are also published with the IMAP-DOAS v6.0 XCH_4 product.

The estimated single-retrieval precision is scene-dependent and averages roughly 1.5 % or 25 ppb (Frankenberg et al., 2011). With this order of instrument precision, SCIAMACHY cannot resolve day-to-day variability of emissions but can strongly constrain a multi-year average (Turner et al., 2015). The retrieving algorithm firstly calculates CH_4 total column density Ω_{CH_4} (molecules cm^{-2}):

$$\Omega_{CH_4} = \Omega_A + \boldsymbol{a}^T(\omega - \omega_A) \quad (1)$$

where ω is the true 10-layer sub-column densities of CH_4 (molecules cm^{-2}), ω_A is the 10-layer prior CH_4 sub-column density (molecules cm^{-2}), Ω_A is the corresponding a priori CH_4 total column density, and $\boldsymbol{a}$ is an averaging kernel vector that defines the sensitivity of the retrieved total column to each sub-column in ω. To account for the impact of aerosol scattering and instrument effects on the observed light path, Frankenberg et al. (2006) used the CO_2 column density Ω_{CO_2} as a proxy to normalize and convert Ω_{CH_4} to a column mixing ratio XCH_4 (ppb):

$$XCH_4 = (\Omega_{CH_4}/\Omega_{CO_2})XCO_2 \quad (2)$$

where XCO_2 is the column-weighted mixing ratio of CO_2. CO_2 is used as a proxy because it is retrieved in a spectrally neighboring fitting window and, relative to CH_4, its mixing ratio is known with much higher precision.

As general retrieval quality deteriorates after November 2005 due to the dysfunction of two important detector pixels (Frankenberg et al., 2011), only observations

ACPD
15, 32469–32518, 2015

during the period of January 2003 to October 2005 are used. The quality of SCIAMACHY observations is controlled by a filtering scheme that selects only daytime, over land and with cloud free or partially cloud scenes and good fitting accuracy (http://www.temis.nl/climate/docs/TEMIS_SCIA_CH4_IMAPv60_PSD_v2_6.pdf). Further, a surface elevation filter is applied to filter out observations that are different from the model grids at surface altitude by more than 250 m (Bergamaschi et al., 2009; Alexe et al., 2015). This filtering process ensures that the atmospheric columns seen by SCIAMACHY are well represented by the model columns. To avoid spurious outliers that may have a large impact on the inversion, XCH_4 retrievals of less than 1500 ppb or larger than 2500 ppb are discarded (Alexe et al., 2015). Figure S1 in the Supplement shows the SCIAMACHY retrievals ($n = 37\,989$) of the weighted column-average CH_4 dry mixing ratio for July 2004–September 2004 in the pan-Arctic that have passed all quality control tests.

2.2 Surface Observations

The NOAA/ESRL Carbon Cycle Cooperative Global Air Sampling Network provides high-precision measurements of surface atmospheric CH_4 dry-air mole fraction (Dlugokencky et al., 2014). CH_4 measurements were calibrated against the WMO X2004 CH_4 standard scale maintained at NOAA (Dlugokencky et al., 2005). Due to the coarse resolution of the GEOS-Chem model, we include only marine and continental background sites and exclude sites that are strongly influenced by sub-grid local sources, as listed in Table S1 in the Supplement. The flask-air samples in the NOAA/ESRL network that were taken from regular ship cruises in Pacific Ocean serve to evaluate simulated surface mixing ratios of global inversions over the remote ocean and downwind the continental sources (Alexe et al., 2015). One Arctic site (Pallas-Sammaltunturi, Finland (PAL)) that was excluded from the assimilation is used to evaluate the nested-grid inversions.

ACPD
15, 32469–32518, 2015

2.3 Aircraft campaign observations

The modeled CH_4 vertical profiles in the troposphere are evaluated by the NOAA/ESRL Carbon Cycle Cooperative Global Air Sampling Network's aircraft program (http://www.esrl.noaa.gov/gmd/ccgg/aircraft/data.html; Sweeney et al., 2015). For the aircraft observations, CH_4 was routinely collected using 0.7 L silicate glass flasks on planned flights with maximum altitude limits of 300–350 hPa. The sampling vertical resolution is up to 400 m in the boundary layer and all samples were analyzed by NOAA/ESRL in Boulder, Colorado. Table S2 lists the locations and profiles used in evaluation.

3 Modeling

Here we describe the prior emissions, forward model, and inversion method used to optimize CH_4 emissions in the pan-Arctic on the basis of SCIAMACHY and NOAA/ESRL observations.

3.1 Wetland and lake CH_4 emissions

CH_4 emissions estimated by the inverse modeling method can be sensitive to the choice of prior wetland CH_4 fluxes (Bergamaschi, 2007). To assess this sensitivity, we use wetland CH_4 emissions simulated by six well-known wetland biogeochemical models (CLM4Me, DLEM, LPJ-Bern, LPJ-WSL, ORCHIDEE and SDGVM) to setup our inverse model. All wetland CH_4 simulations follow the same protocol of WETland and Wetland CH_4 Inter-comparison of Models Project (WETCHIMP) (Melton et al., 2013; Wania et al., 2013). Melton et al. (2013) demonstrated that the difference of these estimates primarily arises from the model distinction in CH_4 biogeochemistry and wetland hydrology. These models estimated that the annual global CH_4 emissions from wetlands during 2004–2005 were in the range of 121.7–278.1 $Tg\,yr^{-1}$ (Fig. 2 and Table 2) and wetland CH_4 emissions are the highest in tropical regions (e.g., Amazon, South-

ACPD
15, 32469–32518, 2015

east Asia and Tropical Africa) where extensive floodplains and warm environment co-exist. In the Arctic, the modeled annual wetland CH_4 emissions during 2004–2005 were in the range of 11.4–25.6 Tg yr^{-1} (Fig. 3 and Table 3), and their spatial distribution was mainly controlled by the modeled or mapped wetland coverage (Melton et al., 2013). As shown in Fig. 3, because of some consistency in simulating wetland hydrology, nearly all models suggest that there were high CH_4 fluxes in West Siberia Lowlands, Finland and Canadian Shield. As our focus is on 2004–2005, we only use one wetland emission scenario from LPJ-WSL in our inverse model during 1993–2003 to construct initial conditions. As presented in Fig. S2, before optimization, this prior wetland scenario gives the best fit between GEOS-Chem modeled CH_4 and GLOBALVIEW-CH_4 (GLOBALVIEW-CH_4, 2009).

The biogeochemical models involved in the WETCHIMP project have not included CH_4 emissions from lakes. As CH_4 emissions from pan-Arctic lakes could be significant (Walter et al., 2006; Tan and Zhuang, 2015a) and have different drivers relative to wetland emissions, e.g. the supply of labile yedoma permafrost carbon (Walter et al., 2006) and water deep mixing (Schubert et al., 2012), it is necessary to include this source into the Arctic CH_4 inventory. Prior CH_4 emissions from pan-Arctic lakes are simulated with a one-dimension process-based lake biogeochemical model (Tan et al., 2015; Tan and Zhuang, 2015a). The bLake4Me model explicitly parameterizes the control of temperature and carbon substrate availability on methanogenesis, the control of temperature and oxygen level on methanotrophy and the transport of gaseous CH_4 by diffusion and ebullition. The model also includes two thermal modules, governing the heat transport and water phase change in both water and sediments column of lakes. A detailed model description and evaluation is given in Tan et al. (2015). Model estimates of CH_4 emissions from all lakes north of 60° N are described by Tan and Zhuang (2015a, b). On average, the estimated CH_4 emissions from pan-Arctic lakes during the studied period are approximately 11 Tg CH_4 yr^{-1}, see Fig. 3.

ACPD
15, 32469–32518, 2015

3.2 GEOS-Chem model

Atmospheric CH_4 mole fractions are simulated by GEOS-Chem v9-01-03 (http://acmg.seas.harvard.edu/geos/index.html), a global 3-D CTM model (Bey et al., 2001). GEOS-Chem could be driven by either GEOS-4 or GEOS-5 meteorological (met) data from NASA's Global Modeling Assimilation Office (GMAO). As GEOS-5 is available only from December 2003, in this study we use GEOS-4 met data from 1993 to 2005 for inverse simulations when only surface measurements are assimilated and GEOS-5 met data from 2004 to 2005 for inverse simulations when both satellite retrievals and surface measurements are assimilated. Both the GEOS-4 and GEOS-5 met data have horizontal resolution of 1/2° latitude × 2/3° longitude and 6 h temporal resolution. There are 55 and 72 hybrid sigma-pressure levels extending from Earth's surface to 0.01 hPa for GEOS-4 and GEOS-5 met data respectively. In contrast to the global GEOS-Chem model, the nested-grid version does not contain algorithms for handling advection near North and South Poles (Lin and Rood, 1996). To avoid polar grid boxes, we crop the native $1/2^\circ \times 2/3^\circ$ resolution GEOS-5 met data to a window region (180° W–180° E and 80–56° N) for the Arctic nested grid. Boundary conditions for nested grid simulations are produced for the same period with GEOS-Chem 4° × 5° resolution global scale forward runs at 3 h intervals.

The GEOS-Chem CH_4 simulation was originally introduced by Wang et al. (2004) and updated by Pickett-Heaps et al. (2011). As described by Wecht et al. (2014), the prior anthropogenic sources, including oil/gas production, coal mining, livestock, waste treatment, rice paddies, biofuel burning and other processes, are extracted from Emission Database for Global Atmospheric Research v4.2 (EDGAR4.2) with $0.1^\circ \times 0.1^\circ$ resolution and no seasonality (European Commission, Joint Research Centre/Netherlands Environmental Assessment Agency, 2009). CH_4 emissions from termites and biomass burning are obtained from the study of Fung et al. (1991) and daily Global Fire Emissions Database Version 3 (GFED3) (van der Werf et al., 2010), respectively. CH_4 emissions from wetlands and lakes are from the model simulations described in Sect. 3.1.

ACPD
15, 32469–32518, 2015

Atmospheric CH_4 is mainly removed by tropospheric oxidation initiated by reaction with tropospheric OH, which was computed using a 3-D OH climatology of monthly average concentrations from a previous simulation of tropospheric chemistry (Park et al., 2004). The global mean pressure-weighted tropospheric OH concentration is 10.8×10^5 molecules cm^{-3}. For minor sinks, CH_4 uptake by upland soils is derived from Fung et al. (1991) and CH_4 oxidation in the stratosphere is calculated from the archived CH_4 loss frequency described by Murray et al. (2012). The resulting atmospheric lifetime of CH_4 is about 8.9 years, consistent with the observational constraint of 9.1 ± 0.9 years (Prather et al., 2012). We regrid and crop the anthropogenic and natural CH_4 emissions in EDGAR4.2, GFED3 and Fung et al. (1991) for the nested Arctic domain using the Harvard-NASA Emissions Component (HEMCO) software (Keller et al., 2014), marked as "other" in Fig. 3. Compared to CH_4 emissions from Arctic wetlands and lakes, these sources are relatively small ($\sim 3.2\,Tg\,yr^{-1}$).

3.3 Inversion method

Atmospheric inversion is a procedure for using observations of atmospheric gases as constraints to estimate surface gas fluxes. The inverse problem can be characterized by solution of

$$\boldsymbol{y} = \mathbf{F}(\boldsymbol{x}) + \varepsilon \tag{3}$$

By applying Bayesian theorem and assuming Gaussian errors, the inverse problem can be solved by minimizing the cost function, $J(\boldsymbol{y})$, that measures the model deviations from both prior assumptions and observations:

$$J(\boldsymbol{x}) = (F(\boldsymbol{x}) - \boldsymbol{y})^T \mathbf{C}_d^{-1} (\mathbf{F}(\boldsymbol{x}) - \boldsymbol{y}) + \gamma (\boldsymbol{x} - \boldsymbol{x}_0)^T \mathbf{C}_{\boldsymbol{x}_0}^{-1} (\boldsymbol{x} - \boldsymbol{x}_0) \tag{4}$$

where $\boldsymbol{y}$ is a vector of observations from SCIAMACHY and NOAA/ESRL, $\mathbf{F}$ is a model operator that maps emissions to observations, $\boldsymbol{y}$ represents CH_4 emissions to be constrained, $\boldsymbol{y}_0$ is the a priori estimate of $\boldsymbol{y}$, $\mathbf{C}_d$ is the observational error covariance matrix

ACPD
15, 32469–32518, 2015

that includes contributions from model error, representation error (sampling mismatch between observations and the model) and measurement error, and $\mathbf{C}_{x_0}$ is the parameter error covariance matrix (containing the uncertainties of the parameters and their correlations). The regularization parameter γ controls the relative constraints applied by the observational and a priori parts of $J(\boldsymbol{y})$ (Kopacz et al., 2009). In the adjoint method, γ is not fixed at unity but determined by analyzing its influence on the minimum of $J(\boldsymbol{y})$ (Henze et al., 2007; Kopacz et al., 2009).

Minimization of $J(\boldsymbol{y})$ yields the following expression for the maximum a posteriori solution for the state vector ($\hat{\boldsymbol{x}}$) and its associated error covariance ($\hat{\boldsymbol{C}}_{\boldsymbol{x}}$) (Rodgers, 2000):

$$\hat{\boldsymbol{x}} = \boldsymbol{x}_0 + \left((\nabla_{\boldsymbol{x}}\mathbf{F})^T \mathbf{C}_d^{-1} \nabla_{\boldsymbol{x}}\mathbf{F} + \gamma \mathbf{C}_{\boldsymbol{x}_0}^{-1}\right)^{-1} (\nabla_{\boldsymbol{x}}\mathbf{F})^T \mathbf{C}_d^{-1} (\boldsymbol{y} - \mathbf{F}(\boldsymbol{x}_0)) \quad (5)$$

$$\hat{\boldsymbol{C}}_{\boldsymbol{x}}^{-1} = (\nabla_{\boldsymbol{x}}\mathbf{F})^T \mathbf{C}_d^{-1} \nabla_{\boldsymbol{x}}\mathbf{F} + \gamma \mathbf{C}_{\boldsymbol{x}_0}^{-1} \quad (6)$$

where $\nabla_{\boldsymbol{x}}\mathbf{F}$ is the Jacobian matrix of the forward model. $J(\boldsymbol{y})$ is minimized iteratively through successive forward and backward simulations with the GEOS-Chem model and its adjoint, developed by Henze et al. (2007) and previously applied to CO, CO_2 and CH_4 source inversions (Jiang et al., 2011; Deng et al., 2014; Wecht et al., 2014). The GEOS-Chem adjoint model is a 4DVAR inverse modeling system that allows optimization of a very large number of parameters using at the same time very large sets of observational data, such as satellite data. Rather than optimizing CH_4 emissions, it optimizes an exponential scale factor $e_{\boldsymbol{x}}$ ($e_{\boldsymbol{x}} = \ln(\boldsymbol{x}/\boldsymbol{x}_0)$) at each grid cell to avoid negative emissions.

For prior emissions, the uncertainties are set as 100 % in each grid box and the spatial correlation is set as an e-folding function with spatial correlation lengths of 500 km at the global coarse resolution ($4^\circ \times 5^\circ$) and of 300 km at the nested grid resolution ($1/2^\circ \times 2/3^\circ$) (Bergamaschi et al., 2009). Optimization is performed in three steps. First, a global coarse-resolution inversion using the LPJ-WSL wetland scenario is run from 1993 to 2005 using surface measurements only. This inversion provides the optimized

ACPD
15, 32469–32518, 2015

CH_4 fields for the calculation of bias correction functions and initial conditions for the next set of inversions. Next, we run six global coarse-resolution inversions using the wetland CH_4 scenarios described in Sect. 3.1 at two time windows: January 2004–December 2004 and July 2004–June 2005. In these global inversions, both surface measurements and satellite retrievals are assimilated. The inverse modeling at the 1st time block servers as a spin-up period and the analysis time period is from July 2004 to June 2005 (Deng et al., 2014; Alexe et al., 2015). Besides optimizing global CH_4 fluxes, the global inversions also provide boundary conditions for our nested grid inversions. Following Turner et al. (2015), we construct time-dependent boundary conditions for the nested simulations of the adjoint model from the forward model at $4^\circ \times 5^\circ$ horizontal resolution using the posterior emissions from a global inversion performed first. This is different from the method of Wecht et al. (2014) where both emissions and boundary conditions were optimized by minimizing two separate cost functions iteratively. The last step is thus to run nested grid inversions in the Arctic at $1/2^\circ \times 2/3^\circ$ resolution to optimize Arctic CH_4 emissions. The modeling period is from 24 June to 1 October 2004 and the real analysis time is from 1 July to 1 October 2004. As in Wecht et al. (2014), observations in the first week are not assimilated. This time period is selected based on two factors. First, due to snow cover and large solar zenith angle, the quality of SCIAMACHY retrievals in winter is usually low. Second, CH_4 fluxes from pan-Arctic wetlands and lakes are the most pronounced in summer. In all steps, optimization is run iteratively at least 40 times until the reduction of the cost function becomes less than 0.5 % with each successive iteration (Wecht et al., 2014).

3.4 Satellite retrieval bias correction

The importance of bias correction to satellite retrievals in inversion of CH_4 fluxes has been emphasized in earlier studies (Bergamaschi et al., 2007, 2009, 2013; Fraser et al., 2013; Cressot et al., 2014; Houweling et al., 2014; Wecht et al., 2014; Alexe et al., 2015; Turner et al., 2015). These methods relied on regression between a proxy parameter (i.e., latitude, air mass factor or specific humidity) and retrieval bias. Air mass factor was

ACPD
15, 32469–32518, 2015

chosen because of the co-variation of spectroscopic errors with the sampled air mass and residual aerosol errors (Cressot et al., 2014; Houweling et al., 2014) and specific humidity was chosen because water vapor is the main cause of SCIAMACHY seasonal bias that lags the variations of solar zenith angle (Houweling et al., 2014). Many studies used seasonal and latitudinally varying functions for bias correction because they can represent the changes in both solar zenith angle and climate variables (Bergamaschi et al., 2007, 2009, 2013). It is likely that retrieval bias can be better represented if the effects of air mass change and climate system change can be accounted for together.

To test this hypothesis, we compare the performances of three traditional one-proxy methods (latitude φ, air mass factor A_F, specific humidity H_S) and two new two-proxy methods (latitude + humidity, air mass factor + humidity), listed in Table 1. After constraining the GEOS-Chem model with surface measurements, the bias correction method that gives the smallest difference between the measured and modeled CH_4 column mixing ratios and the lowest Bayesian Information Criterion (BIC) score will be used. Specific humidity is taken from the European Centre for Medium-Range Weather Forecasts (ECMWF)'s ERA-20C reanalysis product (http://apps.ecmwf.int/datasets/data/era20c-daily), averaged by the column between the surface and 3 km altitude (Houweling et al., 2014). The air mass factor and central latitude of CH_4 retrievals are directly available in the SCIAMACHY IMAP v6.0. For bias correction, we first optimize the GEOS-Chem 4-D CH_4 mixing ratios by an inversion using surface measurements and then sample the modeled XCH_4 at the coordinates and time of SCIAMACHY retrievals and with local averaging kernels applied. The difference between SIAMACHY and GEOS-Chem values (Fig. 1a) is regressed with proxy factors to obtain the optimal bias correction. As suggested by Turner et al. (2015), it is more likely that grid squares between 50° S and 50° N with residual standard deviation (RSD) in excess of 20 ppb are dominated by model bias in prior emissions. Thus, we exclude such grid squares in regressions. Further, satellite retrievals with low precisions (the ratio of retrieval precision error to retrieval is larger than 3 %) are removed from analysis. In our experiments, all bias correction functions are updated monthly. Unlike Bergam-

ACPD
15, 32469–32518, 2015

aschi et al. (2009), we do not further optimize bias correction functions in the inversion cycle because such an optimization could make bias correction account for the uncertainties that should not be dealt with by correction, e.g. unaccounted model errors or even the sources and sinks (Houweling et al., 2014). As listed in Table 1, the "latitude only" correction performs the best within three single proxy correction methods and only slightly worse than the best correction method "latitude + humidity" in our test. This implies that the latitude polynomial correction used in most previous CH_4 inversions is appropriate. As the "latitude + humidity" method performs the best, it is applied for satellite bias correction in this study. After bias correction, we estimated the error variances of SCIAMACHY observations (Fig. 1b) using a relative residual error (RRE) method described by Heald et al. (2004). Figure 1d indicates that the correction greatly reduces model-satellite differences in tropical areas of America, Africa and South Asia and also reduces the difference in Australia and some areas of the United States. As shown in Fig. 1c, the agreement between GEOS-Chem and SCIAMACHY XCH_4 is also improved at the global scale. However, because the model-data difference in East Asia has an opposite latitude dependence to that in other areas of the same latitudes (Fig. 1a), the correction deteriorates the model-satellite agreement there (Fig. 1d).

The observational error of the NOAA/ESRL CH_4 mixing ratios is estimated as the sum of measurement error ($\sim 0.2\,\%$) and representation error. Similar to satellite retrievals, the representation error of surface measurements is defined as the standard deviation of the difference of CH_4 residuals between NOAA/ESRL measurements and GEOS-Chem. And the CH_4 residuals are calculated by subtracting the simulated or observed CH_4 mixing ratios by a fitted polynomial trend (Masarie and Tans, 1995).

ACPD
15, 32469–32518, 2015

4 Results and discussion

4.1 Optimized global CH_4 emissions

As shown in Fig. 4, the posterior global and regional CH_4 emissions exhibit a strong seasonal variability during 1993–2005, which is mainly driven by the sensitivity of methanogenesis in natural sources to temperature (e.g., wetlands). During this period, there are prominently positive CH_4 emission anomalies in 1994 (+27.4 Tg CH_4) and 1998 (+34.6 Tg CH_4), and prominently negative anomalies in 1997 (−18.4 Tg CH_4), 2001 (−20.5 Tg CH_4) and 2005 (−22.3 Tg CH_4). The 1998 CH_4 emission peak has been documented in many studies (e.g., Dlugokencky et al., 2001; Rigby et al., 2008). Dlugokencky et al. (2001) attributed this anomaly to an increase in the imbalance between CH_4 sources and sinks equal to ∼ 24 Tg CH_4, suggested to be caused by an increase of wetland emissions in both tropical regions (13 Tg CH_4) and the Northern Hemisphere (11.6 Tg CH_4) and a severe fire year in boreal regions (5.7 Tg CH_4). However, according to Fig. 4, wetlands only contributed a small amount of emission increase during 1998 (9.1 Tg CH_4) and most of the increase was from other sources (e.g., biomass burning) in both tropical and high-latitude regions. Our findings are consistent with the claim of Langenfelds et al. (2002) that two CH_4 emission pulses in 1994 and 1998 could be linked with large biomass burning events in tropical and boreal regions. During 1993–1996, the annual mean of global CH_4 emissions was 534 Tg CH_4 yr^{-1}, slightly lower than the estimate (549 ± 7 Tg CH_4 yr^{-1}) of Dlugokencky et al. (1998). During 1993–2005, there are no visible trends for wetland emissions in tropical, northern mid-latitude and northern high-latitude regions. Also, the annual mean of global CH_4 emissions did not change between 1993 and 2004, coinciding with the leveling off of CH_4 growth rate since the 1990s (Dlugokencky et al., 1998 & 2003). Kai et al. (2011) claimed that the evolution of CH_4 mixing ratios in the recent decades was a result of long-term reduction in agricultural emissions (i.e. rice paddies) or landfills emissions within the Northern Hemisphere. In Fig. 4b, the long-term decline of CH_4 emissions from tropical non-wetland sources seems to provide some support to this argument. But as the

ACPD
15, 32469–32518, 2015

finding of inter-hemispheric $\delta^{13}CH_4$ is questionable (Levin et al., 2012), it is uncertain whether this declined tropical source is in the Northern Hemisphere.

The posterior global CH_4 emissions using both NOAA/ESRL and SCIAMACHY observations and different prior wetland scenarios are shown in Fig. 5 and also listed in Table 2. Since total emissions are constrained by the atmospheric burden of CH_4 and the CH_4 lifetime, while the prior CH_4 fluxes in six scenarios are different in a wide range of estimates (471.5–627.8 $Tg\,CH_4\,yr^{-1}$), the posterior global CH_4 emissions converge into a very narrow zone (496.4–511.5 $Tg\,CH_4\,yr^{-1}$). This suggests that the surface observations are of sufficient density to constrain the global emissions. However, there are still not enough high-precision measurements at regional scales, resulting in large differences between the posterior emissions in the TransCom3 land regions (Table 2).

There have been many studies that assimilated surface and/or satellite observations into a CTM inverse model to constrain global CH_4 fluxes, see Kirschke et al. (2013) for review. For instance, using the same observations suite, Bergamaschi et al. (2009) estimated that in 2004, CH_4 emissions in global, tropical (30° S–30° N), northern extratropical (30–90° N) and southern extratropical (90–30° S) zonal areas were 506.7, 323.5, 172.8 and 10.4 $Tg\,CH_4\,yr^{-1}$, respectively. These large-scale estimates are consistent with our calculations: 284.5–319.6 $Tg\,CH_4\,yr^{-1}$ (tropical), 165.3–206.6 $Tg\,CH_4\,yr^{-1}$ (northern extratropical) and 10.0–13.9 $Tg\,CH_4\,yr^{-1}$ (southern extratropical). This agreement reflects that GEOS-Chem adjoint and TM5-4DVAR are consistent in the atmospheric transport, chemistry and inverse modeling methods. In contrast to Bergamaschi et al. (2009), our inversions tend to allocate more emissions to extratropical regions. As a result, the tropical total (SATr + NAF + SAF + TrA) of the six inversions is in the range of 114.1–169.7 $Tg\,CH_4\,yr^{-1}$, which is much lower than their estimate of 203.2 $Tg\,CH_4\,yr^{-1}$. The most likely reason for this discrepancy from Bergamaschi et al. (2009) is that we use a much larger correction to the SCIAMACHY data in tropical regions. The posterior CH_4 emissions from wetlands in our four scenarios (Bern, CLM4Me, SDGVM and WSL) are close to the estimate (~ 161 $Tg\,CH_4\,yr^{-1}$) of Bloom

ACPD
15, 32469–32518, 2015

et al. (2010) for 2003–2007 based on CH_4 and gravity spaceborne data to constrain large-scale methanogenesis. Our estimates are also close to the inferred CH_4 emissions ($175 \pm 33\,Tg\,CH_4\,yr^{-1}$) from natural wetlands by Kirschke et al. (2013). By using artificial neural networks, Zhu et al. (2013) estimated that from 1990 to 2009, annual wetland CH_4 emissions from northern high latitudes ($> 45^{\circ}$ N) are in the range of 44.0–$53.7\,Tg\,CH_4\,yr^{-1}$, agreeing with the estimates of the Bern, CLM4Me and SDGVM scenarios.

The renewed growth of atmospheric CH_4 since 2007 has been observed by several studies (Rigby et al., 2008; Dlugokencky et al., 2009; Nisbet et al., 2014). According to Nisbet et al. (2014), the global growth rate was about $6\,ppb\,yr^{-1}$ from 2007 to 2012. Assuming 1 ppb equivalent to $2.75\,Tg\,CH_4$ in the entire atmosphere (Khalil et al., 2007) and the lifetime of atmospheric CH_4 constant, the estimated global CH_4 emissions during 2010–2011 should be at most 49.5 Tg larger than the estimated during 2004–2005. The higher CH_4 emissions after 2007 were also demonstrated by other top-down studies: $539\,Tg\,CH_4\,yr^{-1}$ during 2009–2011 (Turner et al., 2015) and $538 \pm 15\,Tg\,CH_4\,yr^{-1}$ during August 2009–July 2010 (Cressot et al., 2014). When comparing the estimate of Alexe et al. (2015) for 2010–2011 with our estimates (Table 2), the difference is in the range of 29–$44.1\,Tg\,CH_4$ (Table 2), consistent with these independent studies. Our estimates also agree well with the inference of Houweling et al. (2014) that global CH_4 emissions in 2004 were close to $500\,Tg\,CH_4\,yr^{-1}$ and the emissions rose by 27–$35\,Tg\,CH_4\,yr^{-1}$ after July 2006. In contrast, the ensemble Kalman filter assessment in Fraser et al. (2013) involving GOSAT observations and GEOS-Chem is $510.6 \pm 18.4\,Tg\,CH_4\,yr^{-1}$ for the period June 2009–December 2010 (Table 2). They probably underestimated the emissions during this period because the calculated increase from 2004 to 2009 is too low ($\sim 10\,Tg\,CH_4\,yr^{-1}$).

As shown in Fig. 5a, the highest CH_4 fluxes are located in the Amazon, China, Southeast Asia, North America and Europe where extensive wetlands or large population exist. Our inversions indicate that the Eurasian temperate regions, including China, North America and Europe, emitted much more CH_4 than other regions (Table 2), showing

ACPD
15, 32469–32518, 2015

the dominance of anthropogenic sources in the global CH_4 inventory. As presented in Fig. 5c, our inverse model reduces the CH_4 emissions from China, the Amazon basin and Eurasian boreal region (scale factor < 1) but enhances the emissions in Europe and Southeast Asia (scale factor > 1) relative to the prior. This adjustment could be primarily driven by the constraints of the surface measurements and satellite retrievals and secondarily by the satellite bias correction.

4.2 Optimized Arctic CH_4 emissions

In contrast to the global CH_4 inversions, total posterior CH_4 emissions from the Arctic nested-grid inversions span a wide range: 14.6–30.4 $Tg\,CH_4\,yr^{-1}$ (Table 3). It reflects a strong influence from both the priors (Fig. 3) and the nested-grid boundaries (Berchet et al., 2015) on the posteriors (Fig. 6). Across six Arctic inversions, the range of the posterior is not smaller than the range of the prior (25.7–39.9 $Tg\,CH_4\,yr^{-1}$) and the mean departure of the posterior from the prior is 10.1 $Tg\,CH_4\,yr^{-1}$. This divergence implies that due to uncertain boundary conditions (Berchet et al., 2015), the surface and satellite observations in the Arctic cannot provide sufficient constrains to reduce the estimate uncertainty. Further, as presented in Table 3 and Fig. 6, this lack of constraint from the observations mainly occurs in Siberia and causes large uncertainties in the estimates of Siberian wetland CH_4 emissions (2.0–12.7 $Tg\,CH_4\,yr^{-1}$). In comparison with the inverse modeling of Monteil et al. (2013), we estimate that the annual total CH_4 emission from the pan-Arctic (> 60° N) is 29.2–60.8 % of their estimate (50 $Tg\,CH_4\,yr^{-1}$) for CH_4 emissions in the northern high latitudes (> 50° N). Because all inversions estimate lower CH_4 emissions than the priors, it is possible that CH_4 emissions from Arctic wetlands, lakes and other sources are overestimated by the biogeochemistry models and EDGAR dataset. In contrast to other sources, the estimated CH_4 emissions from Arctic lakes are less divergent in the nested-grid inversions except for the ORCHIDEE scenario, as presented in Fig. 7 and Table 3. There are two reasons for this convergence: (1) CH_4 fluxes from lakes are low in those poorly constrained re-

ACPD
15, 32469–32518, 2015

gions, e.g. Northeastern Europe and Central Siberia, and (2) we only use one lake prior scenario in the inversions. The exception of the ORCHIDEE inversion could be explained by that the ORCHIDEE model simulates very high wetland CH_4 fluxes in Canadian Shield, West Siberia Lowlands and East Siberia Coastal Lowlands where high CH_4 fluxes from lakes are also possible (Fig. 3). For CH_4 emissions from Arctic lakes, our estimates, 5.4–7.9 Tg CH_4 yr^{-1}, are close to the lower bound of the estimate (7.1–17.3 Tg CH_4 yr^{-1}) in Bastviken et al. (2011) with upscaling site-level observations. Even if the lake source is reduced, on average, by 40 % by the inversions, the remaining amounts are still much higher than the previous estimate of ~ 4 Tg CH_4 yr^{-1} in Gao et al. (2013). This emphasizes the importance of including pan-Arctic lakes in the carbon cycle. When the ORCHIDEE scenario is excluded, annual CH_4 emissions from lakes in Alaska, northern Canada, northern Europe and northern Siberia are, on average, 1.0, 3.1, 0.6 and 2.8 Tg CH_4 yr^{-1}, respectively. These estimates correspond to 1.2, 5.0, 0.6 and 5.0 Tg CH_4 yr^{-1} in Tan and Zhuang (2015a) without optimization. The posterior CH_4 emissions from lakes in northern Canada are closer to the estimate of 2.6±0.4 Tg CH_4 yr^{-1} in Tan and Zhuang (2015b) because thermokarst lakes in northern Canada can be better identified by a high-resolution landscape evolution model in Tan and Zhuang (2015b) than by coarse-resolution geographic datasets in Tan and Zhuang (2015a). The posterior lake emissions from northern Siberia are much smaller than the modeled (Tan and Zhuang, 2015a, b). There are two possible reasons for the larger estimates of the lake model: (1) the model overestimates thermokarst active zone of yedoma lakes; and (2) four high-flux yedoma lakes that are used for calibration are not good representative of all yedoma lakes. For European lakes, Saarnio et al. (2009) estimated that they are a CH_4 source of 1.48 Tg CH_4 yr^{-1}. This means that CH_4 emissions from lakes in northern Europe (> 60° N) could constitute 40 % of CH_4 emissions from all European lakes. By upscaling site observations to northern Canada, Laurion et al. (2010) found that annual diffusive CH_4 emission from Canadian thaw ponds was 1.0 Tg CH_4. Since ebullition could be much stronger than diffusion in transporting CH_4

ACPD
15, 32469–32518, 2015

(Bastviken et al., 2011), our estimate of 3.1 Tg CH_4 yr^{-1} from Canadian lakes should not be considered a large overestimate, as indicated in Tan and Zhuang (2015b).

In contrast to Arctic wetlands, scientists have not reached a consensus on the importance of Arctic lakes to the global CH_4 cycle because only a limited number of Arctic lakes have been observed and their characteristics (e.g., morphology, eutrophication and carbon input) are more heterogeneous. In this study, as the constraints of observations are limited, we only optimize total CH_4 emission in each grid cell and fix the weight of each source during our inversions. Since wetlands and lakes are usually spatially neighbored, this operation could attribute a fraction of lake emissions incorrectly to wetlands or vice versa. To verify the possibility of large CH_4 emissions from pan-Arctic lakes, we conducted a nested-grid inversion in the Arctic based on the DLEM scenario that did not include CH_4 emissions from lakes as a comparison. The DLEM scenario was chosen because as presented in Fig. 3 its simulated wetland emissions are less spatially overlapped with the simulated lake emissions. This no-lake inversion shows that there are low CH_4 fluxes in the East Siberia Coastal Lowlands, a region with extensive high-flux yedoma lakes (Walter et al., 2006). In comparison with the original test, this no-lake inversion produces a larger mean difference between the observed and simulated posterior SCIAMACHY XCH_4, 27.4 ppb vs. 26.5 ppb. The 0.9 ppb difference is impressive considering the influence of nested-grid model boundaries. For instance, Berchet et al. (2015), even using high-precision surface measurements collected from eight West Siberian Plain sites, only reduced the difference of the observed and simulated posterior GOSAT XCH_4 by 1.5 ppb in a Eurasian-scale inversion. Another sign that SCIAMACHY XCH_4 can be much better represented by including lake emissions is that the no-lake inversion only reduces the simulated prior SCIAMACHY XCH_4 deviation by 0.1 ppb. Thus, the no-lake scenario probably misses some significant CH_4 emissions in the coastal lowlands. Because 56 % of the water-inundated landscapes (i.e., lakes, wetlands and rivers) in this region are lakes (Lehner and Döll, 2004), lakes, especially yedoma lakes, could have contributed a large fraction of the missed CH_4 emissions.

ACPD
15, 32469–32518, 2015

Arctic tundra is regarded as an important source of CH_4 in northern high latitudes. By using process-based models and atmospheric CH_4 observations, McGuire et al. (2012) estimated that Arctic tundra was a source of 25 Tg CH_4 yr^{-1} to the atmosphere during 1990–2006. By using the TM5-4DVAR inverse model with SCIAMACHY and NOAA/ESRL observations, Alexe et al. (2015) estimated that CH_4 emissions from Arctic wetlands were 18.2 Tg CH_4 yr^{-1} for 2010–2011. A similar estimate of 16 ± 5 Tg CH_4 yr^{-1} was also made by Bruhwiler et al. (2014) with using the CarbonTracker-CH_4 assimilation system. Our estimates of 8.8–20.4 Tg CH_4 yr^{-1} encompass the estimates of Alexe et al. (2015) and Bruhwiler et al. (2014) but are lower than that of McGuire et al. (2012). As discussed, the uncertainty mainly arises from CH_4 emissions from Siberian wetlands. Regionally, when the ORCHIDEE scenario is excluded, annual CH_4 emissions from wetlands in Alaska, northern Canada, northern Europe and northern Siberia are, on average, 1.0, 3.3, 4.2 and 5.8 Tg CH_4 yr^{-1}, respectively. The estimated total CH_4 emission from Alaskan wetlands is much lower than the inferred value of 4.1 Tg CH_4 yr^{-1} for the Alaskan Yukon River basin during 1986–2005 using the modeling of process-based CH_4 biogeochemistry and large-scale hydrology (Lu and Zhuang, 2012) and also much lower than the inferred value of 3 Tg CH_4 yr^{-1} for the whole of Alaska (Zhuang et al., 2007). As wetlands in Europe are predominantly located north of 60° N, our estimate of wetland emissions from northern Europe is very close to a European-scale estimate of 3.6 Tg CH_4 yr^{-1} by Saarnio et al. (2009). The posterior CH_4 emissions from Siberian wetlands show a wide range (2.0–12.7 Tg CH_4 yr^{-1}), which are much smaller than the estimate of 21.63 ± 5.25 Tg CH_4 yr^{-1} by Kim et al. (2012) for the annual mean CH_4 emissions from Siberian wetlands during 2005–2010. Assimilating in situ CH_4 measurements collected at 13 Eurasian sites in Siberia, Finland, Mongolia, China and South Korea, Berchet et al. (2015) estimated that CH_4 budget on the West Siberian Plain was 5–28 Tg CH_4 for 2010. It is also larger than our estimate but shows a similar large uncertainty.

ACPD
15, 32469–32518, 2015

4.3 Method evaluation

Figure 8 shows the difference between the modeled and observed CH_4 mixing ratios at NOAA ship board sampling stations and aircraft vertical profile sites under different wetland scenarios before and after the global scale inversions. For most scenarios, inversion improves the representation of CH_4 mixing ratios in GEOS-Chem at both marine and inland boundary layers and free troposphere. Specifically, the CLM4Me scenario performs best in the evaluation by reducing the difference by more than 10 ppb. Because this scenario also produces global and wetland CH_4 fluxes consistent with earlier studies (as described in Sect. 4.1), it is likely that the spatial pattern of CH_4 fluxes simulated by the CLM4Me model is more realistic than the other scenarios at the global scale.

Figure 9 compares the modeled and observed CH_4 mixing ratios at the PAL surface station, in Finland and the PFA aircraft vertical profile site, in Alaska before and after the nested grid inversions. These two stations are near the main CH_4 sources in northern Europe and Alaska, respectively. For PFA, the nested-grid inversions perform better than the nested-grid forward run but do not have clear advantage over the global inversions. The reason for this could be that CH_4 emissions from Alaska can be well constrained by three NOAA/ESRL surface sites in Alaska (BRW, CBA and SHM) and the CH_4 mixing ratios at PFA are representative of the interior of Alaska as was pointed out in Sweeney et al. (2015).

4.4 Further discussion

As described in Sect. 4, there are still several issues limiting the accuracy of our estimates. First, although the stronger zonal and weaker vertical transport characteristics of northern high latitudes is thought to help transport flux information to the pan-Arctic sites (e.g., Shemya, Barrow and Cold Bay), CH_4 sources in some regions of the Arctic, e.g. Siberia, are still poorly constrained by the assimilated measurements. In theory, because surface and aircraft measurements have much lower uncertainties than satel-

ACPD
15, 32469–32518, 2015

lite retrievals, it is possible to refine our estimates by incorporating site measurements near Siberia, such as the Surgut site of National Institute for Environmental Studies (NIES) (Machida et al., 2001). The uncertainty of SCIAMACHY retrievals likely also needs to be revisited. The assumed 1.5 % minimum uncertainty for SCIAMACHY retrievals in this study could be somewhat overestimated (Bergamaschi et al., 2007), which limits their potentials to provide constraints on CH_4 fluxes. The treatment of the SCIAMACHY bias could be an important uncertainty source for our estimates, as suggested by Houweling et al. (2014). Future top-down studies could benefit from a more reasonable bias correction method, even for low bias satellite products, e.g. GOSAT (Alexe et al., 2015).

Second, the attribution of CH_4 fluxes to spatially overlapped sources, e.g. wetlands and lakes, could be a problem for even high-resolution inversions. Carbon isotope measurements ($\delta^{13}CH_4$) are widely used to separate biogenic and geologic CH_4 sources (Langenfelds et al., 2002) but are not useful for two biogenic sources with similar carbon isotope ratios (Walter et al., 2008; Fisher et al., 2011). One possible solution is to constrain the flux ratio of wetlands to lakes using very fine resolution geographical information. For instance, the flux ratio should be well constrained by the area ratio of these two landscapes. Another possible solution is to jointly constrain CO_2 and CH_4 fluxes in a nested-grid inversion. As known, although both wetlands and lakes are CH_4 sources, wetlands are a CO_2 sink and lakes are a CO_2 source (Zhu et al., 2013; Walter Anthony et al., 2014). This opposite correlations of CH_4 and CO_2 emissions could possibly be used to constrain the optimization of the flux ratio in inverse models.

Our Arctic inversions did not include natural CH_4 sources (e.g., CH_4 emissions from subsea permafrost of East Siberian shelf) other than wetlands and lakes in the Arctic. It could lead to more uncertainties in our estimates. But our study also suggests that it is unlikely that CH_4 emissions from sea shelf are as large as 17 $Tg\,CH_4\,yr^{-1}$ as suggested by Shakhova et al. (2013) because the posterior CH_4 emissions from Arctic wetlands are no more than 20.4 $Tg\,CH_4\,yr^{-1}$.

ACPD
15, 32469–32518, 2015

5 Conclusion

In this study, we use a nested-grid high-resolution chemical transport inverse model in the Arctic domain to constrain CH_4 emissions from Arctic wetlands, lakes and anthropogenic sources. The sensitivity of the method to different prior wetland CH_4 fluxes is also tested. When assimilating NOAA/ESRL and SCIAMACHY observations, we estimate that during July 2004–June 2005, global total CH_4 emission is in the range of 496.4–511.5 $Tg\,CH_4\,yr^{-1}$, with wetlands contributing 130.0–203.3 $Tg\,CH_4\,yr^{-1}$. Both of these estimates are consistent with some widely accepted expert assessments. The nested-grid inversions demonstrate that biogeochemical models tend to overestimate CH_4 emissions from natural sources of the Arctic (e.g., wetlands and lakes). The posterior CH_4 emissions from Arctic lakes from July 2004 to June 2005 are 5.4–7.9 $Tg\,CH_4\,yr^{-1}$, a significant contribution to the Arctic CH_4 cycle. CH_4 emissions from lakes in Alaska, northern Canada, northern Europe and northern Siberia, on average, are estimated to be 1.0, 3.1, 0.6 and 2.8 $Tg\,CH_4\,yr^{-1}$, respectively. Except for the emissions from northern Siberia, other estimates are consistent with the lake biogeochemical model simulations. The posterior CH_4 emissions from Arctic wetlands from July 2004 to June 2005 are 8.8–20.4 $Tg\,CH_4\,yr^{-1}$. CH_4 emissions from wetlands in Alaska, northern Canada, northern Europe and northern Siberia are, on average, 1.0, 3.3, 4.2 and 5.8 $Tg\,CH_4\,yr^{-1}$, respectively. The nested-grid inversions indicate that CH_4 emissions from northern Canada, Alaska, Scandinavia and East Siberia Coastal lowlands are better constrained by the inversions than from other Arctic regions, e.g. most of Siberian wetlands. Evaluation with independent datasets shows that the global inversions and the Arctic inversions with a nested approach improve estimates of methane mixing ratios in boundary layer and free troposphere. The high-resolution inversions provide more details about the spatial distribution of methane emissions in the Arctic, which helps understand the CH_4 cycle in this climate sensitive region.

ACPD
15, 32469–32518, 2015

The Supplement related to this article is available online at doi:10.5194/acpd-15-32469-2015-supplement.

Acknowledgements. We would like to thank the WETCHIMP investigators for making their simulations of wetland methane emissions available. We appreciate the help from Guang-Dih Lei and Bhagirath M. Trivedi at NASA and Robert Yantosca at Harvard for processing nested grid GOES-5 met data and the help from Christoph A. Keller at Harvard for processing nested grid emission data by HEMCO. This study is supported through projects funded to Q. Zhuang by the NASA Land Use and Land Cover Change program (NASA-NNX09AI26G), Department of Energy (DE-FG02-08ER64599), the NSF Division of Information and Intelligent Systems (NSF-1028291), and the NSF Carbon and Water in the Earth Program (NSF-0630319). This research is also in part supported by the Director, Office of Science, Office of Biological and Environmental Research of the US Department of Energy under Contract No. DE-AC02-05CH11231 as part of their Earth System Modeling Program. D. K. Henze acknowledges NOAA grant no. NA14OAR4310136. A. J. Turner was supported by a Department of Energy (DOE) Computational Science Graduate Fellowship (CSGF). The supercomputing resource is provided by Rosen Center for Advanced Computing at Purdue University.

References

Alexe, M., Bergamaschi, P., Segers, A., Detmers, R., Butz, A., Hasekamp, O., Guerlet, S., Parker, R., Boesch, H., Frankenberg, C., Scheepmaker, R. A., Dlugokencky, E., Sweeney, C., Wofsy, S. C., and Kort, E. A.: Inverse modelling of CH_4 emissions for 2010–2011 using different satellite retrieval products from GOSAT and SCIAMACHY, Atmos. Chem. Phys., 15, 113–133, doi:10.5194/acp-15-113-2015, 2015.

Aydin, M., Verhulst, K. R., Saltzman, E. S., Battle, M. O., Montzka, S. A, Blake, D. R., Tang, Q., and Prather, M. J.: Recent decreases in fossil-fuel emissions of ethane and methane derived from firn air, Nature, 476, 198–201, 2011.

Bastviken, D., Tranvik, L., Downing, J., Crill, P. M., and Enrich-Prast, A.: Freshwater methane emissions offset the continental carbon sink, Science, 331, 50–50, 2011.

Berchet, A., Pison, I., Chevallier, F., Paris, J.-D., Bousquet, P., Bonne, J.-L., Arshinov, M. Y., Belan, B. D., Cressot, C., Davydov, D. K., Dlugokencky, E. J., Fofonov, A. V., Galanin, A.,

ACPD
15, 32469–32518, 2015

Lavrič, J., Machida, T., Parker, R., Sasakawa, M., Spahni, R., Stocker, B. D., and Winderlich, J.: Natural and anthropogenic methane fluxes in Eurasia: a mesoscale quantification by generalized atmospheric inversion, Biogeosciences, 12, 5393–5414, doi:10.5194/bg-12-5393-2015, 2015.

Bergamaschi, P., Krol, M., Dentener, F., Vermeulen, A., Meinhardt, F., Graul, R., Ramonet, M., Peters, W., and Dlugokencky, E. J.: Inverse modelling of national and European CH_4 emissions using the atmospheric zoom model TM5, Atmos. Chem. Phys., 5, 2431–2460, doi:10.5194/acp-5-2431-2005, 2005.

Bergamaschi, P., Frankenberg, C., Meirink, J. F., Krol, M., Dentener, F., Wagner, T., Platt, U., Kaplan, J. O., Körner, S., Heimann, M., Dlugokencky, E. J., and Goede, A.: Satellite chartography of atmospheric methane from SCIAMACHY on board ENVISAT: 2. Evaluation based on inverse model simulations, J. Geophys. Res., 112, D02304, doi:10.1029/2006JD007268, 2007.

Bergamaschi, P., Frankenberg, C., Meirink, J. F., Krol, M., Villani, M. G., Houweling, S., Dentener, F., Dlugokencky, E. J., Miller, J. B., Gatti, L. V., Engel, A., and Levin, I.: Inverse modeling of global and regional CH_4 emissions using SCIAMACHY satellite retrievals, J. Geophys. Res., 114, D22301, doi:10.1029/2009JD012287, 2009.

Bergamaschi, P., Houweling, S., Segers, A., Krol, M., Frankenberg, C., Scheepmaker, R. A., Dlugokencky, E., Wofsy, S. C., Kort, E. A., Sweeney, C., Schuck, T., Brenninkmeijer, C., Chen, H., Beck, V., and Gerbig, C.: Atmospheric CH_4 in the first decade of the 21st century: Inverse modeling analysis using SCIAMACHY satellite retrievals and NOAA surface measurements, J. Geophys. Res. Atmos., 118, 1–20, doi:10.1002/jgrd.50480, 2013.

Bey, I., Jacob, D. J., Yantosca, R. M., Logan, J. A., Field, B. D., Fiore, A. M., Li, Q., Liu, H. Y., Mickley, L. J., and Schultz, M. G.: Global modeling of tropospheric chemistry with assimilated meteorology: model description and evaluation, J. Geophys. Res., 106, 23073–23095, 2001.

Bloom, A. A., Palmer, P. I., Fraser, A., Reay, D. S., and Frankenberg, C.: Large-scale controls of methanogenesis inferred from methane and gravity spaceborne data, Science, 327, 322–325, doi:10.1038/nchem.467, 2010.

Bousquet, P., Ciais, P., Miller, J. B., Dlugokencky, E. J., Hauglustaine, D. A, Prigent, C., Van der Werf, G. R., Peylin, P., Brunke, E.-G., Carouge, C., Langenfelds, R. L., Lathière, J., Papa, F., Ramonet, M., Schmidt, M., Steele, L. P., Tyler, S. C., and White, J.: Contribution of anthropogenic and natural sources to atmospheric methane variability, Nature, 443, 439–443, doi:10.1038/nature05132, 2006.

ACPD
15, 32469–32518, 2015

Bousserez, N., Henze, D. K., Perkins, A., Bowman, K. W., Lee, M., Liu, J., Deng, F., and Jones, D. B. A.: Improved analysis-error covariance matrix for high-dimensional variational inversions: application to source estimation using a 3-D atmospheric transport model, Q. J. Roy. Meteor. Soc., 141, 1906–1921, doi:10.1002/qj.2495, 2015.

Bruhwiler, L., Dlugokencky, E., Masarie, K., Ishizawa, M., Andrews, A., Miller, J., Sweeney, C., Tans, P., and Worthy, D.: CarbonTracker-CH_4: an assimilation system for estimating emissions of atmospheric methane, Atmos. Chem. Phys., 14, 8269–8293, doi:10.5194/acp-14-8269-2014, 2014.

Butz, A., Hasekamp, O. P., Frankenberg, C., Vidot, J., and Aben, I.: CH_4 retrievals from space-based solar backscatter measurements: performance evaluation against simulated aerosol and cirrus loaded scenes, J. Geophys. Res.-Atmos., 115, D24302, doi:10.1029/2010JD014514, 2010.

Cressot, C., Chevallier, F., Bousquet, P., Crevoisier, C., Dlugokencky, E. J., Fortems-Cheiney, A., Frankenberg, C., Parker, R., Pison, I., Scheepmaker, R. A., Montzka, S. A., Krummel, P. B., Steele, L. P., and Langenfelds, R. L.: On the consistency between global and regional methane emissions inferred from SCIAMACHY, TANSO-FTS, IASI and surface measurements, Atmos. Chem. Phys., 14, 577–592, doi:10.5194/acp-14-577-2014, 2014.

Deng, F., Jones, D. B. A., Henze, D. K., Bousserez, N., Bowman, K. W., Fisher, J. B., Nassar, R., O'Dell, C., Wunch, D., Wennberg, P. O., Kort, E. A., Wofsy, S. C., Blumenstock, T., Deutscher, N. M., Griffith, D. W. T., Hase, F., Heikkinen, P., Sherlock, V., Strong, K., Sussmann, R., and Warneke, T.: Inferring regional sources and sinks of atmospheric CO_2 from GOSAT XCO_2 data, Atmos. Chem. Phys., 14, 3703–3727, doi:10.5194/acp-14-3703-2014, 2014.

Denman, K. L., Brasseur, G., Chidthaisong, A., Ciais, P., Cox, P. M., Dickinson, R. E., Hauglustaine, D., Heinze, C., Holland, E., Jacob, D., Lohmann, U., Ramachandran, S., da Silva Dias, P. L., Wofsy, S. C., and Zhang, X.: Couplings between changes in the climate system and biogeochemistry. in: Climate Change 2007: the Physical Science Basis, contribution of Working Group I to the Fourth Assessment Report of the Intergovernmental Panel on Climate Change, edited by: Solomon, S., Qin, D., Manning, M., Chen, Z., Marquis, M., Averyt, K. B., Tignor, M., and Miller, H. L., Cambridge University Press, Cambridge, UK and New York, NY, USA, 2007.

Dlugokencky, E., Masarie, K., and Lang, P.: Continuing decline in the growth rate of atmospheric methane burden, Nature, 393, 447–450, 1998.

ACPD
15, 32469–32518, 2015

Dlugokencky, E. J., Houweling, S., Bruhwiler, L., Masarie, K. A., Lang, P. M., Miller, J. B, and Tans, P. P.: Atmospheric methane levels off: temporary pause or a new steady-state?, Geophys. Res. Lett., 30, 1992, doi:10.1029/2003GL018126, 2003.

Dlugokencky, E. J., Myers, R. C., Lang, P. M., Masarie, K. A., Crotwell, A. M., Thoning, K. W., Hall, B. D., Elkins, J. W., and Steele, L. P.: Conversion of NOAA atmospheric dry-air CH_4 mole fractions to a gravimetrically prepared standard scale, J. Geophys. Res.-Atmos., 110, D18306, doi:10.1029/2005JD006035, 2005.

Dlugokencky, E. J., Bruhwiler, L., White, J. W. C., Emmons, L. K., Novelli, P. C., Montzka, S. A., Masarie, K. A., Lang, P. M., Crotwell, A. M., Miller, J. B., and Gatti, L. V.: Observational constraints on recent increases in the atmospheric CH_4 burden, Geophys. Res. Lett., 36, L18803, doi:10.1029/2009GL039780, 2009.

Dlugokencky, E. J., Lang, P. M., Crotwell, A. M., Masarie, K. A., and Crotwell, M. J.: Atmospheric Methane Dry Air Mole Fractions from the NOAA ESRL Carbon Cycle Cooperative Global Air Sampling Network, 1983–2013, Version: 24 June 2014, available at: ftp://ftp.cmdl.noaa.gov/data/trace_gases/ch4/flask/surface/ (last access: 9 June 2015), 2014.

Enting, I. G.: Inverse Problems in Atmospheric Constituent Transport, Cambridge University Press, 2002.

Etheridge, D. M., Steele, L. P., Francey, R. J., and Langenfelds, R. L.: Atmospheric methane between 1000 A.D., and present: evidence of anthropogenic emissions and climatic variability, J. Geophys. Res., 103, 15979–15993, 1998.

European Commission, Joint Research Centre/Netherlands Environmental Assessment Agency: Emission Database for Global Atmospheric Research (EDGAR), release version 4.0., available at: http://edgar.jrc.ec.europa.eu (last access: 11 July 2015), 2009.

Fiore, A. M., Horowitz, L. W., Dlugokencky, E. J., and West, J. J.: Impact of meteorology and emissions on methane trends, 1990–2004, Geophys. Res. Lett., 33, L12809, doi:10.1029/2006GL026199, 2006.

Fisher, R. E., Sriskantharajah, S., Lowry, D., Lanoisellé, M., Fowler, C. M. R., James, R. H., Hermansen, O., Lund Myhre, C., Stohl, A., Greinert, J., Nisbet-Jones, P. B. R., Mienert, J., and Nisbet, E. G.: Arctic methane sources: isotopic evidence for atmospheric inputs, Geophys. Res. Lett., 38, L21803, doi:10.1029/2011GL049319, 2011.

Frankenberg, C., Meirink, J. F., Bergamaschi, P., Goede, A. P. H., Heimann, M., Kröner, S., Platt, U., van Weele, M., and Wagner, T.: Satellite chartography of atmospheric methane

ACPD
15, 32469–32518, 2015

from SCIAMACHY on board ENVISAT: analysis of the years 2003 and 2004, J. Geophys. Res., 111, D07303, doi:10.1029/2005JD006235, 2006.

Frankenberg, C., Bergamaschi, P., Butz, A., Houweling, S., Meirink, J. F., Notholt, J., Petersen, A. K., Schrijver, H., Warneke, T., and I. Aben: Tropical methane emissions: a revised view from SCIAMACHY onboard ENVISAT, Geophys. Res. Lett., 35, L15811, doi:10.1029/2008GL034300, 2008.

Frankenberg, C., Aben, I., Bergamaschi, P., Dlugokencky, E. J., van Hees, R., Houweling, S., van der Meer, P., Snel, R., and Tol, P.: Global column-averaged methane mixing ratios from 2003 to 2009 as derived from SCIAMACHY: trends and variability, J. Geophys. Res., 116, D02304, doi:10.1029/2010JD014849, 2011.

Fraser, A., Palmer, P. I., Feng, L., Boesch, H., Cogan, A., Parker, R., Dlugokencky, E. J., Fraser, P. J., Krummel, P. B., Langenfelds, R. L., O'Doherty, S., Prinn, R. G., Steele, L. P., van der Schoot, M., and Weiss, R. F.: Estimating regional methane surface fluxes: the relative importance of surface and GOSAT mole fraction measurements, Atmos. Chem. Phys., 13, 5697–5713, doi:10.5194/acp-13-5697-2013, 2013.

Fung, I., John, J., Lerner, J., Matthews, E., Prather, M., Steele, L. P., and Fraser, P. J.: Three-dimensional model synthesis of the global methane cycle, J. Geophys. Res., 96, 13033–13065, doi:10.1029/91JD01247, 1991.

Gao, X., Schlosser, C. A., Sokolov, A., Walter Anthony, K., Zhuang, Q., and Kicklighter, D.: Permafrost degradation and methane: low risk of biogeochemical climate-warming feedback, Environ. Res. Lett., 8, 035014, doi:10.1088/1748-9326/8/3/035014, 2013.

GLOBALVIEW-CH_4: Cooperative Atmospheric Data Integration Project – Methane. CD-ROM, NOAA ESRL, Boulder, Colorado, available at: ftp://ftp.cmdl.noaa.gov (last access: 19 August 2015), Path: products/globalview/ch4, 2009.

Gurney, K. R., Law, R. M., Denning, A. S., Rayner, P. J., Baker, D., Bousquet, P., Bruhwiler, L., Chen, Y.-H., Ciais, P., Fan, S., Fung, I. Y., Gloor, M., Heimann, M., Higuchi, K., John, J., Maki, T., Maksyutov, S., Masarie, K., Peylin, P., Prather, M., Pak, B. C., Randerson, J., Sarmiento, J., Taguchi, S., Takahashi, T., and Yuen, C.-W.: Towards robust regional estimates of CO_2 sources and sinks using atmospheric transport models, Nature, 415, 626–630, doi:10.1038/415626a, 2002.

Heald, C. L., Jacob, D. J., Jones, D. B. A., Palmer, P. I., Logan, J. A., Streets, D. G., Sachse, G. W., Gille, J. C., Hoffman, R. N., and Nehrkorn, T.: Comparative inverse analy-

ACPD
15, 32469–32518, 2015

sis of satellite (MOPITT) and aircraft (TRACE-P) observations to estimate Asian sources of carbon monoxide, J. Geophys. Res., 109, D23306, doi:10.1029/2004JD005185, 2004.
Henze, D. K., Hakami, A., and Seinfeld, J. H.: Development of the adjoint of GEOS-Chem, Atmos. Chem. Phys., 7, 2413–2433, doi:10.5194/acp-7-2413-2007, 2007.
Houweling, S., Krol, M., Bergamaschi, P., Frankenberg, C., Dlugokencky, E. J., Morino, I., Notholt, J., Sherlock, V., Wunch, D., Beck, V., Gerbig, C., Chen, H., Kort, E. A., Röckmann, T., and Aben, I.: A multi-year methane inversion using SCIAMACHY, accounting for systematic errors using TCCON measurements, Atmos. Chem. Phys., 14, 3991–4012, doi:10.5194/acp-14-3991-2014, 2014.
Jiang, Z., Jones, D. B. A., Kopacz, M., Liu, J., Henze, D. K., and Heald, C.: Quantifying the impact of model errors on top-down estimates of carbon monoxide emissions using satellite observations, J. Geophys. Res., 116, D15306, doi:10.1029/2010JD015282, 2011.
Kai, F. M., Tyler, S. C., Randerson, J. T., and Blake, D. R.: Reduced methane growth rate explained by decreased Northern Hemisphere microbial sources, Nature, 476, 194–197, doi:10.1038/nature10259, 2011.
Kaminski, T. and Heimann, M.: Inverse modeling of atmospheric carbon dioxide fluxes, Science, 294, 259–259, 2001.
Keller, C. A., Long, M. S., Yantosca, R. M., Da Silva, A. M., Pawson, S., and Jacob, D. J.: HEMCO v1.0: a versatile, ESMF-compliant component for calculating emissions in atmospheric models, Geosci. Model Dev., 7, 1409–1417, doi:10.5194/gmd-7-1409-2014, 2014.
Khalil, M. A. K., Butenhoff, C. L., and Rasmussen, R. A.: Atmospheric methane: trends and cycles of sources and sinks, Environ. Sci. Technol., 41, 2131–2137, 2007.
Kim, H., Machida, T., Sasakawa, M., Belikov, D., Saeki, T., Ito, A., and Maksyutov, S.: Recent variation of Siberian CH_4 fluxes estimated from atmospheric observations of CH_4, AGU Fall Meeting Abstracts, 1, GC24A-08, 2012.
Kirschke, S., Bousquet, P., Ciais, P., Saunois, M., Canadell, J. G., Dlugokencky, E. J., Bergamaschi, P., Bergmann, D., Blake, D. R., Bruhwiler, L., Cameron-Smith, P., Castaldi, S., Chevallier, F., Feng, L., Fraser, A., Heimann, M., Hodson, E. L., Houweling, S., Josse, B., Fraser, P. J., Krummel, P. B., Lamarque, J.-F., Langenfelds, R. L., Le Quéré, C., Naik, V., O'Doherty, S., Palmer, P. I., Pison, I., Plummer, D., Poulter, B., Prinn, R. G., Rigby, M., Ringeval, B., Santini, M., Schmidt, M., Shindell, D. T., Simpson, I. J., Spahni, R., Steele, L. P., Strode, S. A., Sudo, K., Szopa, S., van der Werf, G. R., Voulgarakis, A., van Weele, M., Weiss, R. F., Williams,

ACPD
15, 32469–32518, 2015

J. E., and Zeng, G.: Three decades of global methane sources and sinks, Nat. Geosci., 6, 813–823, doi:10.1038/ngeo1955, 2013.
Kopacz, M., Jacob, D. J., Henze, D. K., Heald, C. L., Streets, D. G., and Zhang, Q.: Comparison of adjoint and analytical Bayesian inversion methods for constraining Asian sources of carbon monoxide using satellite (MOPITT) measurements of CO columns, J. Geophys. Res., 114, D04305, doi:10.1029/2007JD009264, 2009.
Kort, E. A., Wofsy, S. C., Daube, B. C., Diao, M., Elkins, J. W., Gao, R. S., Hintsa, E. J., Hurst, D. F., Jimenez, R., Moore, F. L., Spackman, J. R., and Zondlo, M. A.: Atmospheric observations of Arctic Ocean methane emissions up to 82° north, Nat. Geosci., 5, 1–4, doi:10.1038/ngeo1452, 2012.
Koven, C. D., Ringeval, B., Friedlingstein, P., Ciais, P., Cadule, P., Khvorostyanov, D., Krinner, G., and Tarnocai, C.: Permafrost carbon-climate feedbacks accelerate global warming, P. Natl. Acad. Sci. USA, 108, 14769–14774, doi:10.1073/pnas.1103910108, 2011.
Langenfelds, R. L., Francey, R. J., Pak, B. C., Steele, L. P., Lloyd, J., Trudinger, C. M., and Allison, C. E.: Interannual growth rate variations of atmospheric CO_2 and its $\delta^{13}C$, H_2, CH_4, and CO between 1992 and 1999 linked to biomass burning, Global Biogeochem. Cy., 16, 1048, doi:10.1029/2001GB001466, 2002.
Laurion, I., Vincent, W., MacIntyre, S., Retamal, L., Dupont, C., Francus, P., and Pienitz, R.: Variability in greenhouse gas emissions from permafrost thaw ponds, Limnol. Oceanogr., 55, 115–133, doi:10.4319/lo.2010.55.1.0115, 2010.
Lehner, B. and Döll, P.: Development and validation of a global database of lakes, reservoirs and wetlands, J. Hydrol., 296, 1–22, 2004.
Levin, I., Veidt, C., Vaughn, B. H., Brailsford, G., Bromley, T., Heinz, R., Lowe, D., Miller, J. B., Poß, C., and White, J. W. C.: No inter-hemispheric $\delta^{13}CH_4$ trend observed, Nature, 486, E3–E4, doi:10.1038/nature11175, 2012.
Lin, S.-J. and Rood, R. B.: Multidimensional flux-form semi-Lagrangian transport schemes, Mon. Weather Rev., 124, 2046–2070, 1996.
Lu, X. and Zhuang, Q.: Modeling methane emissions from the Alaskan Yukon River basin, 1986–2005, by coupling a large-scale hydrological model and a process-based methane model, J. Geophys. Res., 117, G02010, doi:10.1029/2011JG001843, 2012.
Machida, T., Nakazawa, T., Muksyutov, S., Tohjima, Y., Takahashi, Y., Watai, T., Vinnichenko, N., Panchenko, M., Arshinov, M., Fedoseev, N., and Inoue, G.: Temporal and spatial variations

ACPD
15, 32469–32518, 2015

of atmospheric CO_2 mixing ratio over Siberia, paper presented at the Sixth International CO_2 Conference, Sendai, Japan, 1–5, 2001.

Masarie, K. A. and Tans, P. P.: Extension and integration of atmospheric carbon dioxide data into a globally consistent measurement record, J. Geophys. Res., 100, 11593–11610, doi:10.1029/95JD00859, 1995.

McGuire, A. D., Christensen, T. R., Hayes, D., Heroult, A., Euskirchen, E., Kimball, J. S., Koven, C., Lafleur, P., Miller, P. A., Oechel, W., Peylin, P., Williams, M., and Yi, Y.: An assessment of the carbon balance of Arctic tundra: comparisons among observations, process models, and atmospheric inversions, Biogeosciences, 9, 3185–3204, doi:10.5194/bg-9-3185-2012, 2012.

Meirink, J. F., Bergamaschi, P., and Krol, M. C.: Four-dimensional variational data assimilation for inverse modelling of atmospheric methane emissions: method and comparison with synthesis inversion, Atmos. Chem. Phys., 8, 6341–6353, doi:10.5194/acp-8-6341-2008, 2008.

Melton, J. R., Wania, R., Hodson, E. L., Poulter, B., Ringeval, B., Spahni, R., Bohn, T., Avis, C. A., Beerling, D. J., Chen, G., Eliseev, A. V., Denisov, S. N., Hopcroft, P. O., Lettenmaier, D. P., Riley, W. J., Singarayer, J. S., Subin, Z. M., Tian, H., Zürcher, S., Brovkin, V., van Bodegom, P. M., Kleinen, T., Yu, Z. C., and Kaplan, J. O.: Present state of global wetland extent and wetland methane modelling: conclusions from a model inter-comparison project (WETCHIMP), Biogeosciences, 10, 753–788, doi:10.5194/bg-10-753-2013, 2013.

Meng, L., Paudel, R., Hess, P. G. M., and Mahowald, N. M.: Seasonal and interannual variability in wetland methane emissions simulated by CLM4Me' and CAM-chem and comparisons to observations of concentrations, Biogeosciences, 12, 4029–4049, doi:10.5194/bg-12-4029-2015, 2015.

Miller, S. M., Wofsy, S. C., Michalak, A. M., Kort, E. A., Andrews, A. E., Biraud, S. C., Dlugokencky, E. J., Eluszkiewicz, J., Fischer, M. L., Janssens-Maenhout, G., Miller, B. R., Miller, J. B., Montzka, S. A., Nehrkorn, T., and Sweeney, C.: Anthropogenic emissions of methane in the United States, P. Natl. Acad. Sci. USA, 110, 20018–20022, doi:10.1073/pnas.1314392110, 2013.

Miller, S. M., Worthy, D. E. J., Michalak, A. M., Wofsy, S. C., Kort, E. A., Havice, T. C., Andrews, A. E., Dlugokencky, E. J., Kaplan, J. O., Levi, P. J., Tian, H., and Zhang, B.: Observational constraints on the distribution, seasonality, and environmental predictors of North American boreal methane emissions, Global Biogeochem. Cy., 28, 146–160, doi:10.1002/2013GB004580, 2014.

ACPD
15, 32469–32518, 2015

Monteil, G., Houweling, S., Butz, A., Guerlet, S., Schepers, D., Hasekamp, O., Frankenberg, C., Scheepmaker, R., Aben, I., and Röckmann, T.: Comparison of CH_4 inversions based on 15 months of GOSAT and SCIAMACHY observations, J. Geophys. Res.-Atmos., 118, 1–17, doi:10.1002/2013JD019760, 2013.

Murray, L. T., Jacob, D. J., Logan, J. A., Hudman, R. C., and Koshak, W. J.: Optimized regional and interannual variability of lightning in a global chemical transport model constrained by LIS/OTD satellite data, J. Geophys. Res., 117, D20307, doi:10.1029/2012JD017934, 2012.

Myhre, G., Shindell, D., Bréon, F.-M., Collins, W., Fuglestvedt, J., Huang, J., Koch, D., Lamarque, J.-F., Lee, D., Mendoza, B., Nakajima, T., Robock, A., Stephens, G., Takemura, T., and Zhang, H.: Anthropogenic and natural radiative forcing, in: Climate Change 2013: the Physical Science Basis, contribution of Working Group I to the Fifth Assessment Report of the Intergovernmental Panel on Climate Change, edited by: Stocker, T. F., Qin, D., Plattner, G.-K., Tignor, M., Allen, S. K., Boschung, J., Nauels, A., Xia, Y., Bex, V., and Midgley, P. M., Cambridge University Press, Cambridge, UK and New York, NY, USA, 2013.

Nisbet, E. G., Dlugokencky, E. J., and Bousquet, P.: Methane on the rise – again, Science, 343, 493–495, doi:10.1126/science.1247828, 2014.

Park, R. J., Jacob, D. J., Field, B. D., Yantosca, R. M., and Chin, M.: Natural and transboundary pollution influences on sulfate-nitrate-ammonium aerosols in the United States: implications for policy, J. Geophys. Res., 109, D15204, doi:10.1029/2003JD004473, 2004.

Parker, R., Boesch, H., Cogan, A., Fraser, A., Feng, L., Palmer, P. I., Messerschmidt, J., Deutscher, N., Griffith, D. W. T., Notholt, J., Wennberg, P. O., and Wunch, D.: Methane observations from the Greenhouse Gases Observing SATellite: comparison to ground-based TCCON data and model calculations, Geophys. Res. Lett., 38, L15807, doi:10.1029/2011GL047871, 2011.

Pickett-Heaps, C. A., Jacob, D. J., Wecht, K. J., Kort, E. A., Wofsy, S. C., Diskin, G. S., Worthy, D. E. J., Kaplan, J. O., Bey, I., and Drevet, J.: Magnitude and seasonality of wetland methane emissions from the Hudson Bay Lowlands (Canada), Atmos. Chem. Phys., 11, 3773–3779, doi:10.5194/acp-11-3773-2011, 2011.

Prather, M. J., Holmes, C. D., and Hsu, J.: Reactive greenhouse gas scenarios: systematic exploration of uncertainties and the role of atmospheric chemistry, Geophys. Res. Lett., 39, L09803, doi:10.1029/2012gl051440, 2012.

Rigby, M., Prinn, R. G., Fraser, P. J., Simmonds, P. G., Langenfelds, R. L., Huang, J., Cunnold, D. M., Steele, L. P., Krummel, P. B., Weiss, R. F., O'Doherty, S., Salameh, P. K.,

ACPD
15, 32469–32518, 2015

Wang, H. J., Harth, C. M., Mühle, J., and Porter, L. W.: Renewed growth of atmospheric methane, Geophys. Res. Lett., 35, L22805, doi:10.1029/2008GL036037, 2008.
Rodgers, C. D.: Inverse Methods for Atmospheric Sounding: Theory and Practice, Vol. 2, edited by: Rodgers, C. D., World Scientific Publishing Co. Pte. Ltd., Singapore, 2000.
Saarnio, S., Winiwarter, W., and Leitão, J.: Methane release from wetlands and watercourses in Europe, Atmos. Environ., 43, 1421–1429, doi:10.1016/j.atmosenv.2008.04.007, 2009.
Schubert, C. J., Diem, T., and Eugster, W.: Methane emissions from a small wind shielded lake determined by eddy covariance, flux chambers, anchored funnels, and boundary model calculations: a comparison, Environ. Sci. Technol., 46, 4515–4522, 2012.
Schuur, E. A. G., McGuire, A. D., Schädel, C., Grosse, G., Harden, J. W., Hayes, D. J., Hugelius, G., Koven, C. D., Kuhry, P., Lawrence, D. M., M.Natali, S., Olefeldt, D., Romanovsky, V. E., Schaefer, K., Turetsky, M. R., Treat, C. C., and Vonk, E. J.: Climate change and the permafrost carbon feedback, Nature, 520, 171–179, doi:10.1038/nature14338, 2015.
Shakhova, N., Semiletov, I., Leifer, I., Sergienko, V., Salyuk, A., Kosmach, D., Chernykh, D., Stubbs, C., Nicolsky, D., Tumskoy, V., and Gustafsson, Ö.: Ebullition and storm-induced methane release from the East Siberian Arctic Shelf, Nat. Geosci., 7, 64–70, doi:10.1038/ngeo2007, 2013.
Shindell, D. T., Faluvegi, G., Koch, D. M., Schmidt, G. A., Unger, N., and Bauer, S. E.: Improved attribution of climate forcing to emissions, Science, 326, 716–718, 2009.
Simpson, I. J., Sulbaek Andersen, M. P., Meinardi, S., Bruhwiler, L., Blake, N. J., Helmig, D., Rowland, F. S., and Blake, D. R.: Long-term decline of global atmospheric ethane concentrations and implications for methane, Nature, 488, 490–494, doi:10.1038/nature11342, 2012.
Singh, K., Jardak, M., Sandu, A., Bowman, K., Lee, M., and Jones, D.: Construction of non-diagonal background error covariance matrices for global chemical data assimilation, Geosci. Model Dev., 4, 299–316, doi:10.5194/gmd-4-299-2011, 2011.
Sweeney, C., Karion, A., Wolter, S., Newberger, T., Guenther, D., Higgs, J. A., Andrews, A. E., Lang, P. M., Neff, D., Dlugokencky, E., Miller, J. B., Montzka, S. A., Miller, B. R., Masarie, K. A., Biraud, S. A., Novelli, P. C., Crotwell, M., Crotwell, A. M., Thoning, K., and Tans, P. P.: Seasonal climatology of CO_2 across North America from aircraft measurements in the NOAA/ESRL Global Greenhouse Gas Reference Network, J. Geophys. Res.-Atmos., 120, 5155–5190, doi:10.1002/2014JD022591, 2015.

ACPD
15, 32469–32518, 2015

Tan, Z. and Zhuang, Q.: Arctic lakes are continuous methane sources to the atmosphere under warming conditions, Environ. Res. Lett., 10, 054016, doi:10.1088/1748-9326/10/5/054016, 2015a.
Tan, Z. and Zhuang, Q.: Methane emissions from pan-arctic lakes during the 21st century: an analysis with process-based models of lake evolution and biogeochemistry, in review, 2015b.
Tan, Z., Zhuang, Q., and Walter Anthony, K.: Modeling methane emissions from arctic lakes: model development and site-level study, J. Adv. Model. Earth Syst., 7, 459–483, doi:10.1002/2014MS000314, 2015.
Tarnocai, C., Canadell, J. G., Schuur, E. A. G., Kuhry, P., Mazhitova, G., and Zimov, S.: Soil organic carbon pools in the northern circumpolar permafrost region, Global Biogeochem. Cy., 23, GB2023, doi:10.1029/2008GB003327, 2009.
Thompson, R. L., Stohl, A., Zhou, L. X., Dlugokencky, E., Fukuyama, Y., Tohjima, Y., Kim, S.-Y., Lee, H., Nisbet, E. G., Fisher, R. E., Lowry, D., Weiss, R. F., Prinn, R. G., O'Doherty, S., Young, D., and White, J. W. C.: Methane emissions in East Asia for 2000–2011 estimated using atmospheric Bayesian inversion, J. Geophys. Res.-Atmos., 120, 4352–4369, doi:10.1002/2014JD022394, 2015.
Turner, A. J., Jacob, D. J., Wecht, K. J., Maasakkers, J. D., Lundgren, E., Andrews, A. E., Biraud, S. C., Boesch, H., Bowman, K. W., Deutscher, N. M., Dubey, M. K., Griffith, D. W. T., Hase, F., Kuze, A., Notholt, J., Ohyama, H., Parker, R., Payne, V. H., Sussmann, R., Sweeney, C., Velazco, V. A., Warneke, T., Wennberg, P. O., and Wunch, D.: Estimating global and North American methane emissions with high spatial resolution using GOSAT satellite data, Atmos. Chem. Phys., 15, 7049–7069, doi:10.5194/acp-15-7049-2015, 2015.
van der Werf, G. R., Randerson, J. T., Giglio, L., Collatz, G. J., Mu, M., Kasibhatla, P. S., Morton, D. C., DeFries, R. S., Jin, Y., and van Leeuwen, T. T.: Global fire emissions and the contribution of deforestation, savanna, forest, agricultural, and peat fires (1997–2009), Atmos. Chem. Phys., 10, 11707–11735, doi:10.5194/acp-10-11707-2010, 2010.
Walter, K. M., Zimov, S. A., Chanton, J. P., Verbyla, D., and Chapin III, F. S.: Methane bubbling from Siberian thaw lakes as a positive feedback to climate warming, Nature, 443, 71–75, doi:10.1038/nature05040, 2006.
Walter, K. M., Smith, L. C., and Chapin III, F. S.: Methane bubbling from northern lakes: present and future contributions to the global methane budget, Philos. T. Roy. Soc. A, 365, 1657–1676, doi:10.1098/rsta.2007.2036, 2007.

ACPD
15, 32469–32518, 2015

Wang, J. S., Logan, J. L., McElroy, M. B., Duncan, B. N., Megretskaia, I. A., and Yantosca, R. M.: 3-D model analysis of the slowdown and interannual variability in the methane growth rate from 1988 to 1997, Global Biogeochem. Cy., 18, GB3011, doi:10.1029/2003GB002180, 2004.

Wania, R., Melton, J. R., Hodson, E. L., Poulter, B., Ringeval, B., Spahni, R., Bohn, T., Avis, C. A., Chen, G., Eliseev, A. V., Hopcroft, P. O., Riley, W. J., Subin, Z. M., Tian, H., van Bodegom, P. M., Kleinen, T., Yu, Z. C., Singarayer, J. S., Zürcher, S., Lettenmaier, D. P., Beerling, D. J., Denisov, S. N., Prigent, C., Papa, F., and Kaplan, J. O.: Present state of global wetland extent and wetland methane modelling: methodology of a model inter-comparison project (WETCHIMP), Geosci. Model Dev., 6, 617–641, doi:10.5194/gmd-6-617-2013, 2013.

Wecht, K. J., Jacob, D. J., Frankenberg, C., Jiang, Z., and Blake, D. R.: Mapping of North American methane emissions with high spatial resolution by inversion of SCIAMACHY satellite data, J. Geophys. Res.-Atmos., 119, 7741–7756, doi:10.1002/2014JD021551, 2014.

Zhu, X., Zhuang, Q., Qin, Z., Glagolev, M., and Song, L.: Estimating wetland methane emissions from the northern high latitudes from 1990 to 2009 using artificial neural networks, Global Biogeochem. Cy., 27, 1–13, doi:10.1002/gbc.20052, 2013.

Zhuang, Q., Melillo, J. M., Kicklighter, D. W., Prinn, R. G., McGuire, A. D., Steudler, P. A., Felzer, B. S., and Hu, S.: Methane fluxes between terrestrial ecosystems and the atmosphere at northern high latitudes during the past century: A retrospective analysis with a process-based biogeochemistry model, Global Biogeochem. Cy., 18, GB3010, doi:10.1029/2004GB002239, 2004.

Zhuang, Q., Melillo, J. M., Sarofim, M. C., Kicklighter, D. W., McGuire, A. D., Felzer, B. S., Sokolov, A., Prinn, R. G., Steudler, P. A., and Hu, S.: CO_2 and CH_4 exchanges between land ecosystems and the atmosphere in northern high latitudes over the 21st century, Geophys. Res. Lett., 33, L17403, doi:10.1029/2006GL026972, 2006.

Zhuang, Q., Melillo, J. M., McGuire, A. D., Kicklighter, D. W., Prinn, R. G., Steudler, P. A., Felzer, B. S., and Hu, S.: Net emissions of CH_4 and CO_2 in Alaska: implications for the region's greenhouse gas budget, Ecol. Appl., 17, 203–212, 2007.

ACPD
15, 32469–32518, 2015

Table 1. Summary of bias correction methods and of mean absolute satellite-model difference (ppb) for 2003–2005 before and after applying bias correction. ΔBIC is the BIC score increase of a bias correction method when referring to the latitude only method.

	Bias correction function*	Mean absolute difference	ΔBIC
No correction		9.271	
Latitude only	$p_0 + p_1\varphi + p_2\varphi^2$	6.305	
Air mass factor only	$p_0 + p_1 A_F$	7.071	161
Humidity only	$p_0 + p_1 H_S$	6.786	73
Latitude + Humidity	$p_0 + p_{11}\varphi + p_{12}\varphi^2 + p_{21} H_S$	6.230	−7
Air mass factor + Humidity	$p_0 + p_{11} A_F + p_{21} H_S$	6.396	12

* p_0, p_1, p_2, p_{11}, p_{12} and p_{21} are regression parameters.

ACPD
15, 32469–32518, 2015

Table 2. Estimated annual CH_4 emissions (units: $Tg\,CH_4\,yr^{-1}$) for TransCom 3 land regions (NAB: North American Boreal, NAT: North American Temperate, SATr: South American Tropical, SAT: South American Temperate, NAf: Northern Africa, SAf: Southern Africa, ErB: Eurasian Boreal, ErT: Eurasian Temperate, TrA: Tropical Asia, Aus: Australasia, and Eur: Europe). The priors are the range of the initial CH_4 emissions given by the six scenarios.

Region	Priors	Posterior						Fraser	Alexe
		Bern	CLM4Me	DLEM	ORCHIDEE	SDGVM	WSL	et al. (2013)	et al. (2015)
NAB	7.9–26.0	24.3	16.2	16.8	27.4	12.0	20.7	5.1 ± 1.1	10.3
NAT	38.5–59.2	33.2	32.8	42.8	49.2	51.2	39.7	62.5 ± 4.4	45.6
SATr	29.6–100.0	43.0	60.8	31.4	61.0	62.3	42.1	49.6 ± 6.4	71.8
SAT	29.1–55.8	31.2	27.1	35.2	39.1	25.6	30.5	55.8 ± 9.5	40.2
NAf	26.8–31.2	34.0	41.3	27.9	28.0	27.7	32.0	46.9 ± 7.3	50.6
SAf	16.0–27.0	18.4	16.2	19.0	24.2	15.6	18.7	36.6 ± 5.8	42.0
ErB	11.5–32.7	19.2	14.3	16.5	18.7	22.2	14.9	16.5 ± 3.8	15.4
ErT	114.9–133.5	97.0	84.9	146.1	92.7	98.3	99.8	115.9 ± 7.3	109.6
TrA	33.1–45.8	47.3	51.4	35.8	33.1	36.4	45.1	43.5 ± 3.2	76.8
Aus	5.8–8.3	7.3	7.7	6.6	7.9	6.3	7.3	17.6 ± 2.7	4.3
Eur	43.6–53.5	54.9	52.2	46.4	43.5	56.5	54.1	39.6 ± 3.7	28.9
Wetlands	121.7–278.1	166.8	164.6	130.0	203.3	161.8	160.7	192.1 ± 16.1	169
Global	471.5–627.8	501.0	497.7	511.5	511.0	496.4	502.9	510.6 ± 18.4	540.5

ACPD
15, 32469–32518, 2015

Table 3. Summary of the prior and posterior CH_4 emissions ($Tg\,CH_4\,yr^{-1}$) from the Arctic from Jul 2004 to Jun 2005. The priors are the range of the initial CH_4 emissions given by the six scenarios.

	Priors	Posterior					
		Bern	CLM4Me	DLEM	ORCHIDEE	SDGVM	WSL
Alaska	2.8–3.9	3.3	2.5	2.2	2.6	1.8	2.3
Northern Canada	6.2–12.4	7.2	9.0	6.9	5.2	4.4	4.3
Northern Europe	5.6–9.7	8.5	5.8	4.8	4.6	6.7	7.5
Northern Siberia	7.0–18.0	8.2	12.7	3.8	2.0	7.2	8.8
Arctic total	25.7–39.9	27.8	30.4	18.1	14.6	20.3	20.0
Wetlands	11.4–25.6	18.7	20.4	9.2	8.8	12.5	10.9
Lakes	11.1	7.7	7.9	7.5	5.4	7.0	7.7
Other	3.2	1.4	2.1	1.4	0.3	0.9	1.4

ACPD
15, 32469–32518, 2015

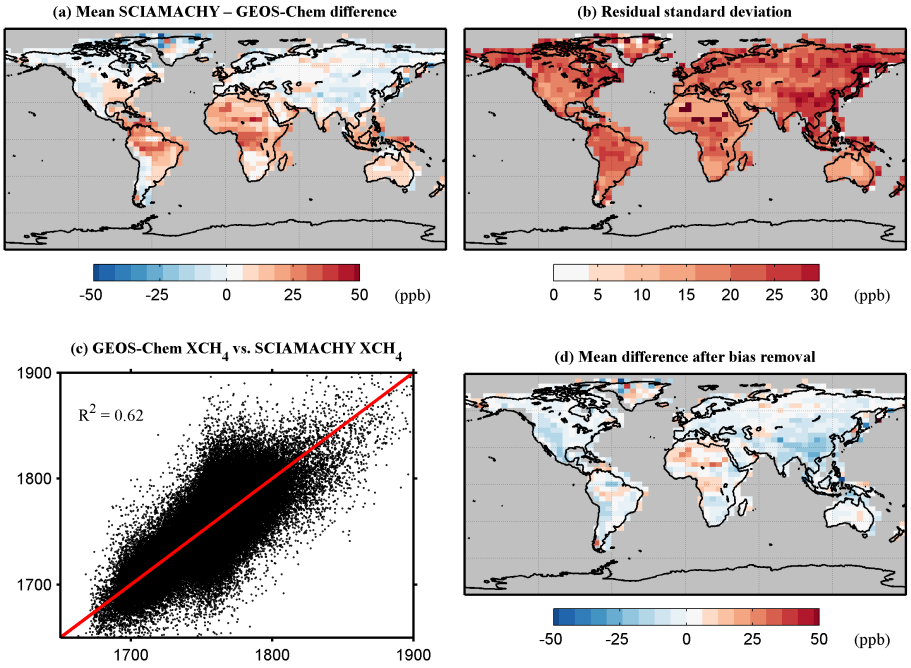

Figure 1. Comparison of column averaged CH_4 mole fractions from SCIAMACHY with those from GEOS-Chem model calculated with prior emissions. **(a, b)** show the mean bias and residual standard deviation of the satellite-model difference, **(c)** shows the comparison of the model (x axis) and satellite (y axis) XCH_4 after applying the "latitude + humidity" correction from the linear regression (weighted R^2 is shown inset and the red 1 : 1 line is also shown), and **(d)** shows the satellite-model difference after bias removal.

ACPD
15, 32469–32518, 2015

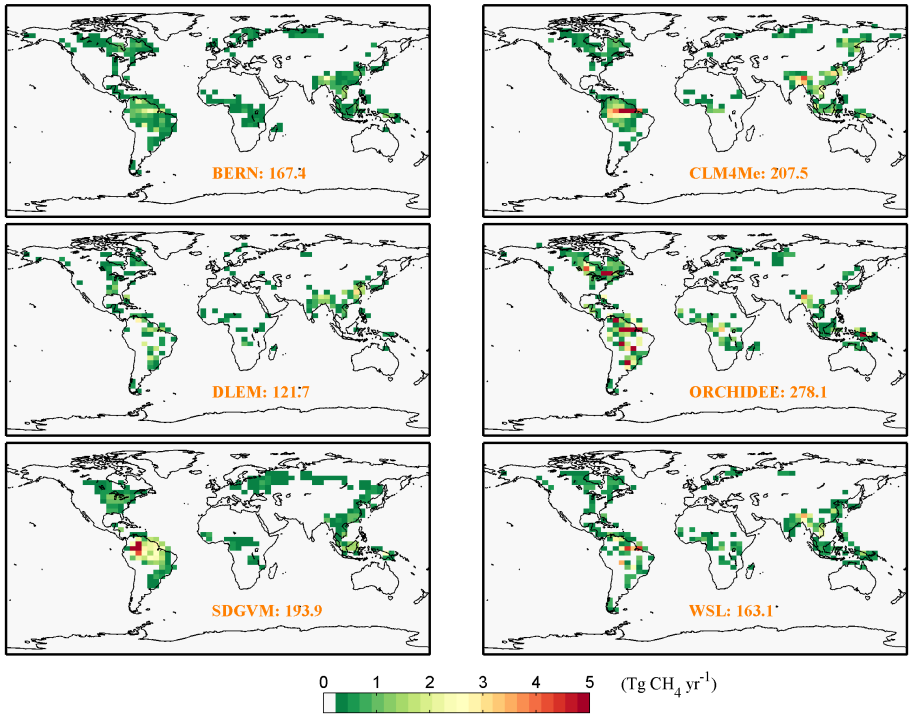

Figure 2. Prior average wetland CH_4 emissions during 2004–2005 from different wetland biogeochemical models used for the GEOS-Chem global inversion at $4^\circ \times 5^\circ$ resolution. Annual total emission (orange) is presented in units of $Tg\,CH_4\,yr^{-1}$.

ACPD
15, 32469–32518, 2015

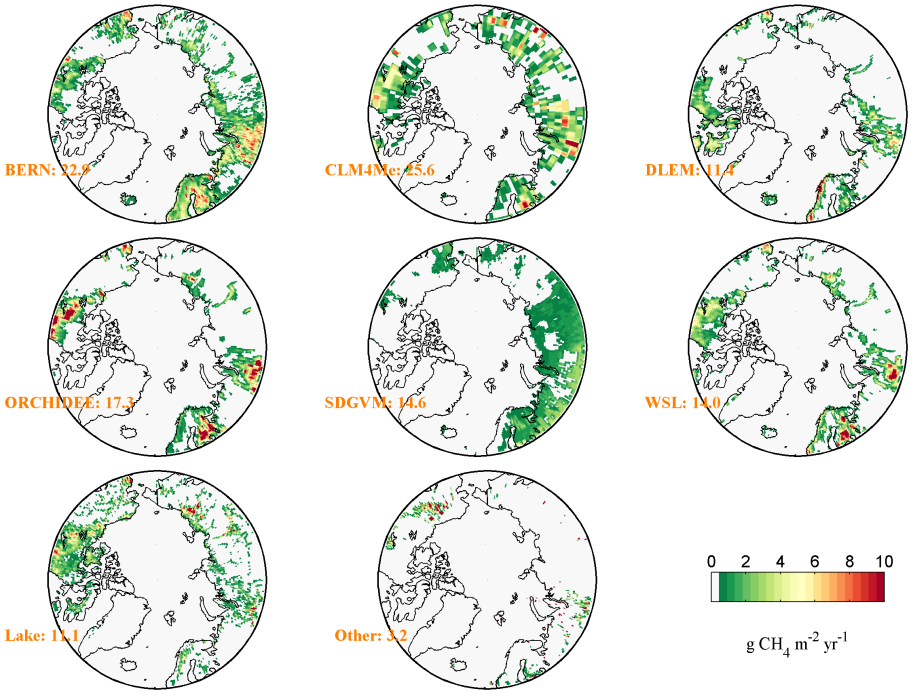

Figure 3. Prior average CH_4 fluxes from wetlands, lakes and other sources (i.e. anthropogenic and biomass burning) during 2004–2005 used in the GEOS-Chem Arctic nested grid inversion at $1/2^\circ \times 2/3^\circ$ resolution. Annual total emission (orange) is presented in units of $Tg\,CH_4\,yr^{-1}$.

ACPD
15, 32469–32518, 2015

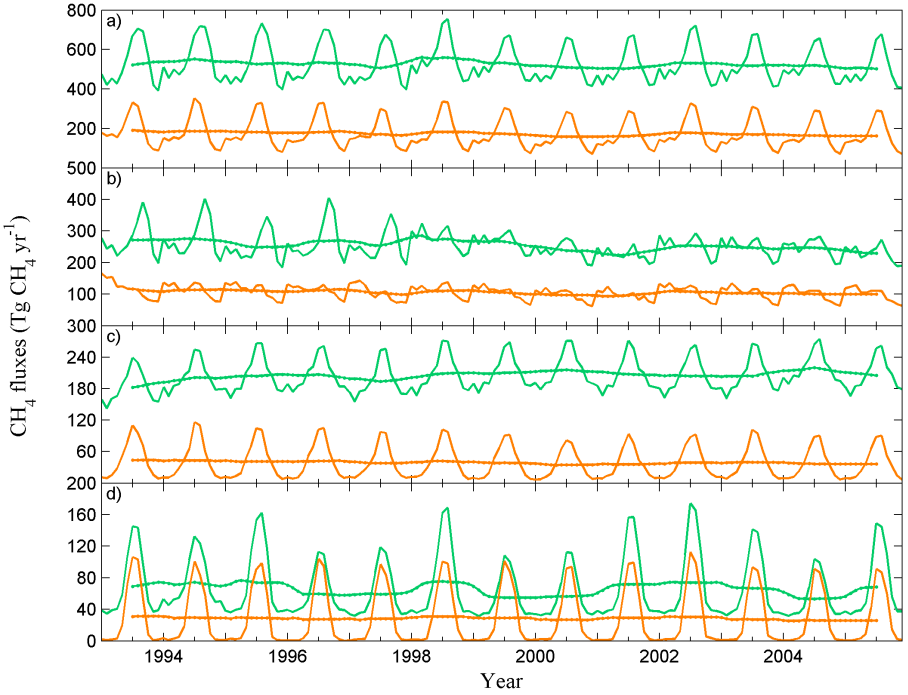

Figure 4. Optimized total (green) and wetlands (orange) CH_4 emissions from 1993 to 2005 by assimilating NOAA/ESRL measurements for **(a)** global, **(b)** tropics (30° S–20° N), **(c)** northern mid-latitude (20–50° N) and **(d)** northern high-latitude (> 50° N). The smooth lines indicate the 12-month average of total and wetlands CH_4 fluxes. The prior wetland CH_4 fluxes are simulated by LPJ-WSL.

ACPD
15, 32469–32518, 2015

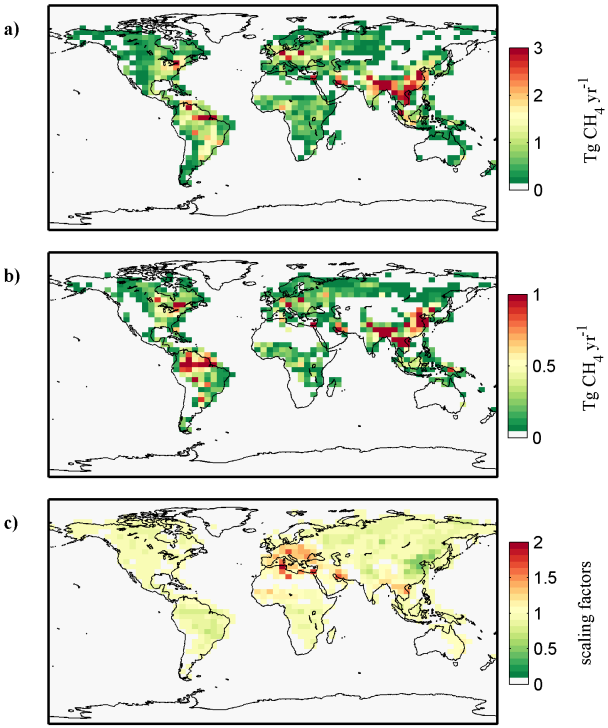

Figure 5. Optimized global CH_4 emissions and emissions scale factors (posterior emissions relative to prior emissions) in the period of July 2004 to June 2005 at 4°×5° resolution using both SCIAMACHY and NOAA/ESRL observations. **(a)** The posterior CH_4 emissions averaged over six inversions; **(b)** the standard deviation of the posterior CH_4 emissions over six inversions; **(c)** the optimized scale factor averaged over six inversions.

ACPD
15, 32469–32518, 2015

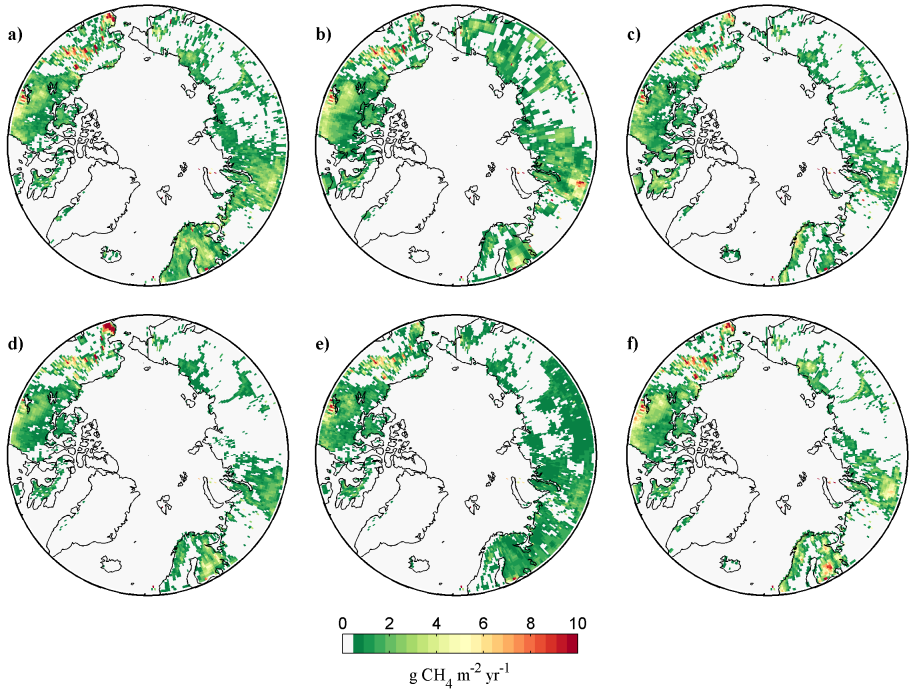

Figure 6. Optimized Arctic CH_4 fluxes from July 2004 to June 2005 at $1/2^\circ \times 2/3^\circ$ resolution using both SCIAMACHY and NOAA/ESRL observations. **(a)** BERN; **(b)** CLM4Me; **(c)** DLEM; **(d)** ORCHIDEE; **(e)** SDGVM; **(f)** WSL.

ACPD
15, 32469–32518, 2015

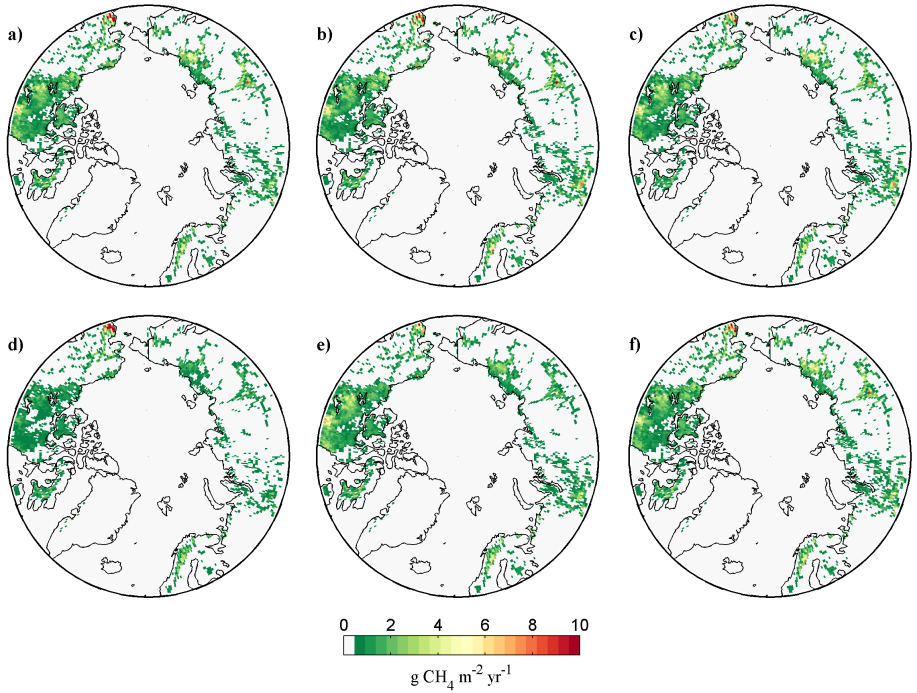

Figure 7. Optimized CH_4 emissions from Arctic lakes from July 2004 to June 2005 at $1/2^\circ \times 2/3^\circ$ resolution using both SCIAMACHY and NOAA/ESRL observations. **(a)** BERN; **(b)** CLM4Me; **(c)** DLEM; **(d)** ORCHIDEE; **(e)** SDGVM; **(f)** WSL.

ACPD
15, 32469–32518, 2015

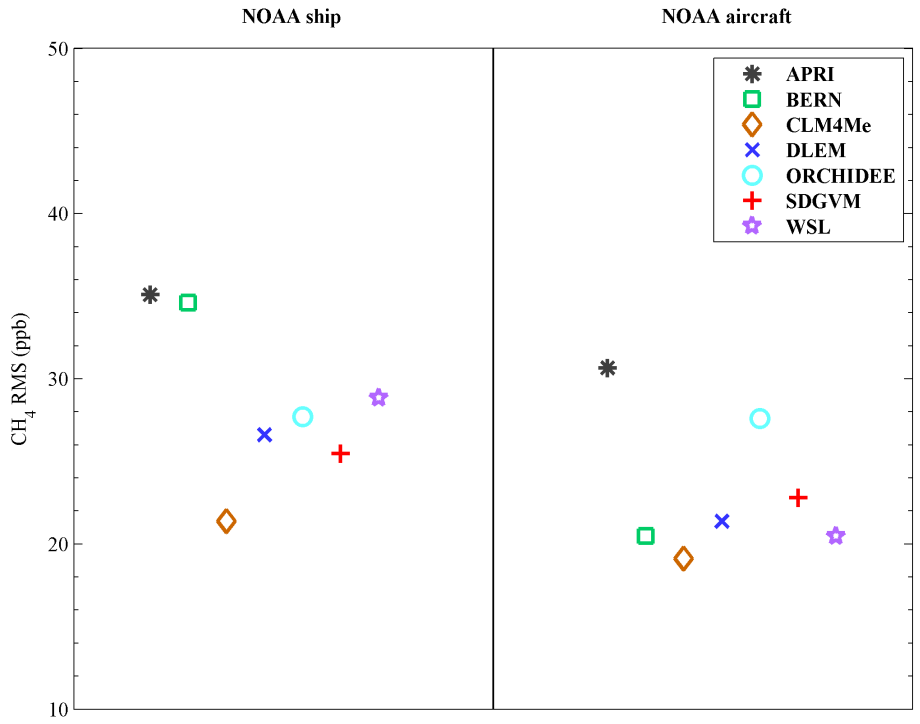

Figure 8. Evaluation of the posterior GEOS-Chem CH_4 mole fractions from the global inversions with independent data sets. The plot shows the root mean square (rms) of differences between modeled and observed CH_4 mixing ratios. APRI indicates the average rms using different prior wetland emissions.

ACPD
15, 32469–32518, 2015

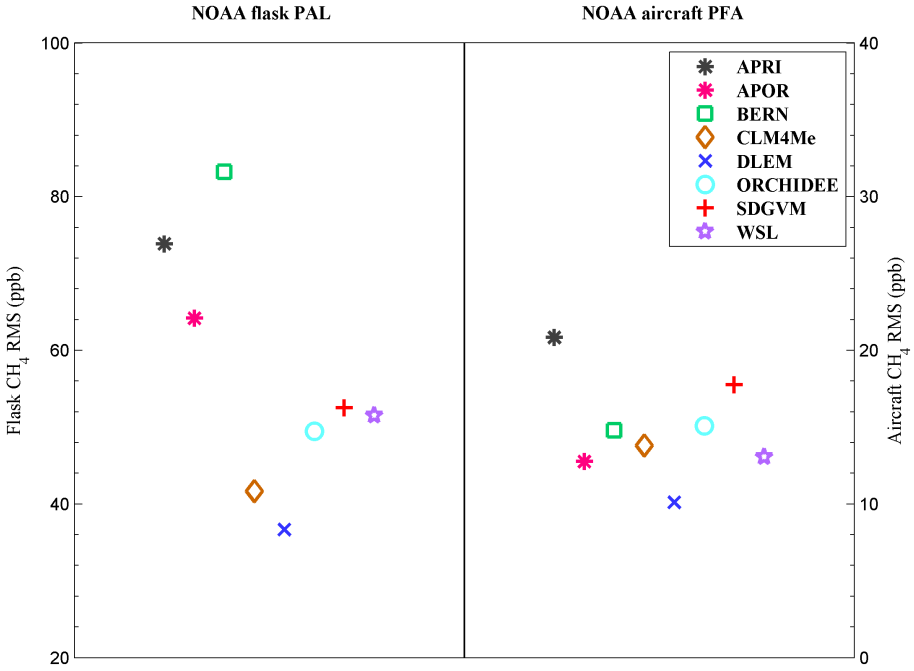

Figure 9. Evaluation of the posterior GEOS-Chem CH_4 mole fractions from the Arctic nested-grid inversions with independent data sets from the NOAA PAL station and the NOAA aircraft PFA profiles. APRI indicates the average rms using different prior wetland emissions. APOR indicates the average rms calculated from six global inversions.

ACPD
15, 32469–32518, 2015